Photoionization of atomic Ca in the 26—120-eV photon-energy range

J. M. Bizau, P. Gérard, and F. J. Wuilleumier
Laboratoire de Spectroscopie Atomique et Ionique, Université de Paris—Sud, Bâtiment 350, F-91405 Orsay, France
and Laboratoire pour l'Utilisation du Rayonnement Electromagnétique, Université de Paris—Sud
Bâtiment 209D, F-91405 Orsay, France

G. Wendin
Institute of Theoretical Physics, Chalmers University of Technology, S-412 96 Göteborg, Sweden
(Received 3 October 1986)

We present detailed experimental results for the resonance structure of atomic Ca in the region of the $3p$ threshold, from 26 to 40 eV, as manifested in the partial cross sections of the $4s^{-1}$ and $3p^{-1}$ main photoelectron lines and several of their satellites, including satellite—to—main-line branching ratios. We also present partial photoionization cross sections for the $4s^{-1}$, $3p^{-1}$, and $3s^{-1}$ main lines up to 120 eV photon energy. Finally, we give a qualitative, theoretical discussion of the resonance structure and decay mechanisms, and compare the measured $4s$, $3p$, and $3s$ photoionization cross sections with theoretical results within the framework of random-phase approximation and many-body perturbation theory.

I. INTRODUCTION

Atomic calcium is the simplest closed-shell atomic system that shows a *full range of many-electron effects.* Since atomic Ca has the ground-state configuration $[\mathrm{Ar}]4s^2$, several types of many-electron effects are similar to what is found for Ar. The unique thing about Ca is the presence of a very "soft" outermost $4s^2$ valence shell, which tends to collapse and "shatter" upon core ionization and give rise to a very rich satellite spectrum. Atomic Ca is therefore a key element for comparing atomic theory with experiment.

The softness of the $4s^2$ shell is due to low-lying empty $3d$ levels. In the presence of a core hole these $3d$ levels become corelike and move down to the vicinity of the $4s$ level. As a consequence, the $3p^5 4s^2$, $3p^5 4s 3d$, and $3p^5 3d^2$ configurations become nearly degenerate and sometimes strongly mixed, leading to pronounced satellite structure both on the low- (shakedown) and high- (shakeup) binding-energy sides of the $3p^5 4s^2$ main photoelectron (PE) lines.

Low-lying, corelike $3d$ levels actually play an important role for most of the strong many-electron effects in Ca. These have been briefly discussed in previous papers,[1,2] and may be summarized as follows.

(i) Screening of the external electromagnetic field by polarization of the $3p$ subshell (collective effects; $3p^{-1}3d,nd,\epsilon d$ electron-hole exchange effects;[1,2] see also Ref. 3). This screening strongly affects the $4s$-, $3p$-, and $3s$-subshell photoionization cross sections in Ca.

(ii) Configuration interaction of the type $3s^{-1} \rightarrow 3p^{-2}3d,nd,\epsilon d$ [giant-Coster-Kronig (gCK)],[4] providing the main mechanism for $3s^{-1}$ relaxation and for generation of intense $3s$ satellites.

(iii) Collapse and breakup of the $4s^2$ shell ($4s \rightarrow 3d$; $4s^2 \rightarrow 3d^2$) upon core ionization or excitation, leading to $3p^{-1}$ shakedown and shakeup satellites and to multielectron satellites in $3p^{-1}nl$ excitations.[1-2,4]

(iv) Auger decay of $3p$ holes, $3p^{-1} \rightarrow 4s^{-2}\epsilon_A$. This process also leads to a rich structure of Auger satellites connected with the $3p^{-1}$ core-hole satellite structure.[2]

(v) Ground-state (initial-state) configuration interaction $4s^2 \rightarrow 3d^2$, $4s^2 \rightarrow 4p^2$. This is the major source of $4s^{-1}$ satellites below the $3p$-excitation-ionization region. It also represents an important element in core ionization [point (iii) above].

The photoelectron spectra in Figs. 1 and 2 illustrate many of the general features. In Fig. 1 the photon energy lies about 3 eV above the principal $3p$ thresholds, in a region with at least doubly excited resonances, and in the vicinity of the thresholds of a group of $3p$ satellites. This leads to a very prominent spectrum of highly excited $4s$ PE satellites, which smoothly goes over into an Auger spectrum above the $Ca^{2+}(3p^6)$ threshold. This Auger-electron (AE) spectrum originates from the $3p^{-1}$ core-hole levels giving rise to the $3p$ PE spectrum extending from about 3 to 6 eV on the kinetic energy scale in Fig. 1.

Figure 1 and, in particular, Fig. 2 clearly demonstrate the close connection between PE and AE spectra. The $4s$ satellite region goes smoothly over into the Auger region when one crosses the Ca^{2+} threshold. Lines close to the threshold, on both sides, will be affected by post-collision-interaction effects (PCI).[3] In the present case there is a one-to-one (mirror image) correspondence between the $3p$ PE and AE spectra. Therefore, the integrated spectrum from 6 eV to, say, 25 eV on the binding-energy scale represents to a good approximation the *absorption* at photon energy $h\nu = 37.66$ eV (we have then neglected the contribution from direct double ionization between 25 and 37.66 eV on the binding-energy scale). The part from 6 to 18 eV represents Ca^{1+} final state while the part between 18 and 25 eV represents Ca^{2+} final states

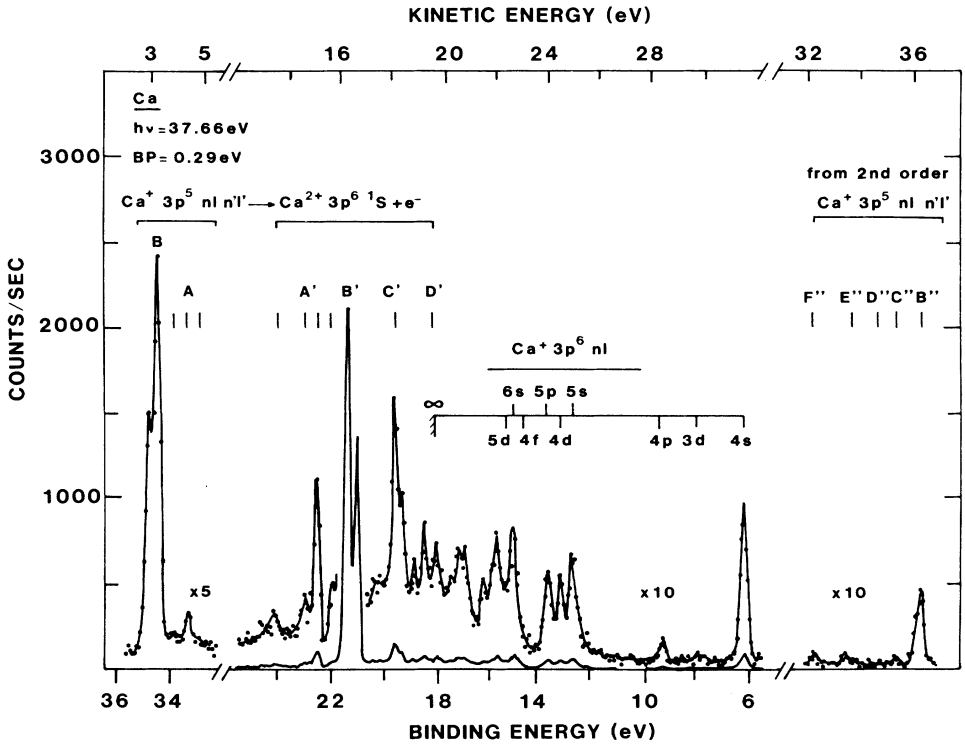

FIG. 1. Spectrum of electrons ejected from atomic calcium by 37.66- and 75.32-eV photons. Peaks A and B (between 3 and 6 eV kinetic energy) and B'' to F'' (32—40 eV) are photoelectrons corresponding to various final states of $3p$-core ionized Ca^{1+} ions, produced by photons diffracted in first order (37.66 eV) and in second order (75.32 eV) by the monochromator. Peaks A'—D' are Auger electrons emitted in the decay of the $3p$-core ionized Ca^{1+} atoms. Peaks labeled $3p^6nl$ are produced by photoionization of Ca atoms in the outer shell; some of the peaks are resonantly enhanced at this photon energy.

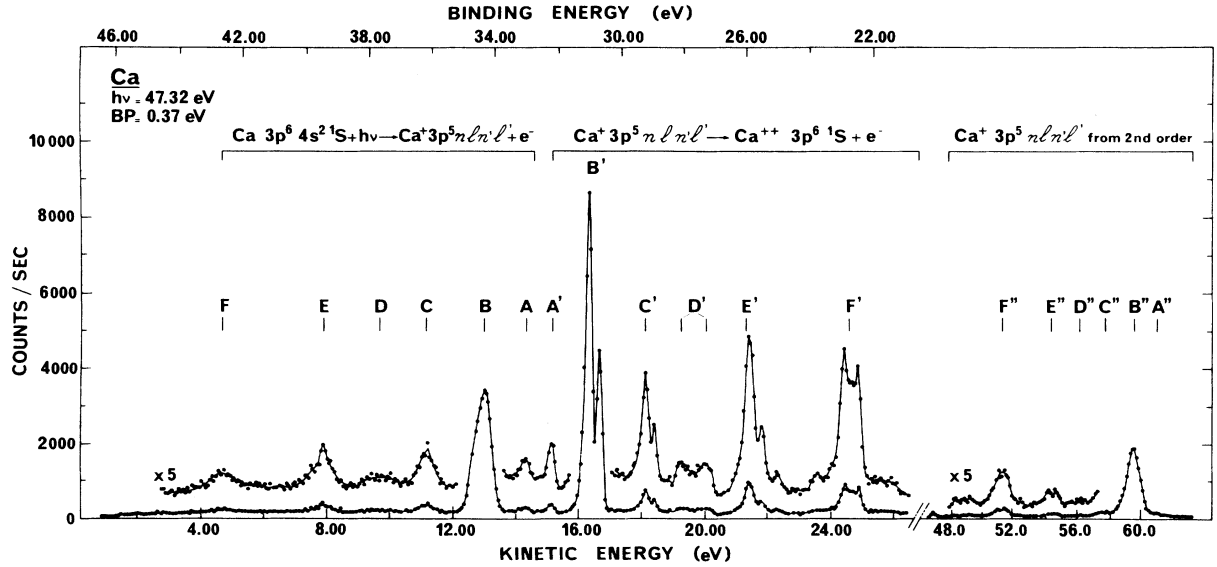

FIG. 2. Electron spectrum following photoionization of atomic calcium by 47.32- and 94.64-eV photons. Labeling of the peaks is the same as in Fig. 1. Photoelectron lines arising from photoionization in the outer shell are not shown here.

from direct and, mainly, two-step double ionization (PE + AE).

In Fig. 2 we show a typical photoelectron spectrum, obtained at a photon energy of 47.32 eV, where the photon energy has been raised to an energy region where there are no strong resonance or threshold effects. The major spectral features are (a) a main $3p^5 4s^2$ ($3p^{-1}$) (spin-orbit split) photoelectron line (B); (b) $3p^5 nlnl'$ shakedown (A) and shakeup (C–F) satellite lines; (c) Auger lines (A' to F') arising from the decay of the corresponding $3p$ holes. The lines labeled A''–F'' are due to photoionization in the $3p$ subshell by photons diffracted in second order by the monochromator (94.64 eV photon energy).

In Fig. 2 the mirror-image relation of the $3p^{-1}$ PE and AE spectra[1,2,5] is obvious, if one takes into account (i) the low transmission of the electron spectrometer at low kinetic energies, (ii) the width of the AE spectrum determined by the resolution of the electron spectrometer (0.2 eV), and (iii) the width of the PE peaks, mainly determined by the bandpass of the photon monochromator (0.4 eV). Strictly speaking, photons diffracted in higher orders by the monochromator also contribute to the intensity of the Auger lines; however, this contribution is small, and its variation over a narrow photon-energy range has been neglected in the present work when using the Auger spectrum to determine the $3p$ photoionization cross section.

Due to its interesting many-electron properties, in recent years atomic Ca has been the subject of several other detailed experimental[6–12] and theoretical[13–19] investigations in addition to the present one.[1,2,20,21] Some of these investigations are of particular importance for the present work: The photoabsorption study by Mansfield and Newsom[7] will serve as reference for identifying single-, double-, and triple-electron resonances in neutral Ca; the analysis of ejected-electron spectra[10] by Mansfield and Ottley[8] will serve as reference for identifying $Ca^{1+}(3p^{-1})$ satellite levels; finally, the photon-energy dependence of the Ca^{1+} and Ca^{2+} photoion yield spectra and branching ratios of Sato *et al.*[12] will be compared with the photon-energy dependence of the main-line and satellite photoelectron and Auger electron spectra and branching ratios of this work.

The many-electron dynamics of atomic Ca in the $3p$ region is closely related to that of atomic Ba in the $5p$ region.[5,22] The spectrum of Ba is, however, much more complicated due to the very strong configuration interaction and large spin-orbit splitting of the $5p^{-1}$ levels.[4,5,23] For comparison with the present experimental work on Ca we would like to draw attention to the recent work on atomic Ba by Bizau *et al.*,[24] Kobrin *et al.*,[25] and Cubaynes *et al.*[26] on photoelectron spectroscopy, and by Holland, Codling, and Chamberlin[27] and Lewandowski *et al.*[28] on photoion yields. Also there is the very recent work by Bizau *et al.*[29] and Cubaynes *et al.*[26] on photoionization of laser-excited Ba.

In general, ESSR (electron spectroscopy with synchrotron radiation) has proven a powerful tool for exploring the electronic structure and dynamics of atoms. Since the pioneering work on the rare gases[30,31] and the first investigations on metallic vapors,[32,33] this technique is now widely used in studies of ionization and decay processes in atoms, molecules, and solids. Regarding metal vapors, especially relevant in the context of this paper are the recent experimental investigations of the transition elements,[34–36] Ga,[37] Ag,[38] Eu,[39] Yb,[40] and Pb.[41,42]

Finally, we should mention the related experimental and theoretical work on valence-band emission of metallic Ca in the region of the $3p$ threshold by Wendin[2(a)] and Barth *et al.*,[43] and the recent electron-energy-loss study of Ca vapor by Ziezel.[44]

In this paper we present extensive results of an experimental and theoretical investigation of the photoionization spectrum of atomic calcium in the $4s$, $3p$, and $3s$ regions.[1,20,21] We have measured the photon-energy dependence of the $4s$, $3p$, and $3s$ main photoelectron lines and many of their satellites and associated Auger lines. The experimental results cover the range from 26 eV to 120 eV and provide a unique material for testing atomic theory.

The plan of the paper is as follows. In Sec. II we describe the experimental procedure and the data analysis, and discuss different possibilities for normalizing cross sections to theoretical calculations. In Sec. III we outline a theoretical framework for treating resonance excitations and decay processes, necessary for interpreting the experimental results. The $4s$, $3p$, and $3s$ main-line photoionization cross sections are presented and discussed in Sec. IV, while the $4s$ and $3p$ satellite cross sections are given in Secs. V and VI, respectively.

II. EXPERIMENTAL PROCEDURE AND DATA TREATMENT

A. Experimental setup

We used our previously described experimental apparatus at the ACO (les Anneaux de Collision du Laboratoire de l'Accélerateur Linéaire, Orsay, France) synchrotron-radiation facility.[45] Synchrotron radiation was monochromatized by a 1-m grazing incidence toroidal grating monochromator.[46] Typically, with a current of 100 mA in ACO at 536 MeV, a flux of 10^{12} photons/sec in 1% band pass was available at the exit slit of the monochromatic in the range 20–140 eV. In this work we have used the lowest band pass of 0.03–0.08 eV in the 26–35-eV region, and a bandpass of about 1% of the photon energy at higher energy. The monochromatized light was refocused by a toroidal mirror into the source volume located on the axis of a cylindrical mirror analyzer (CMA). The CMA accepted electrons emitted from the source volume at the "magic angle" (54°44′). This arrangement makes the measured intensities of the electron signals independent of the polarization of the synchrotron light and of the angular distribution of photoelectrons.[47] The width of the slit of the analyzer may be changed to adjust its resolution. For these experiments, a constant resolution of 0.9% of the kinetic energy of the electrons was adopted.

The Ca vapor was produced in a stainless-steel effusion furnace mounted on the axis of the CMA (Fig. 3). The heating was assured by a Ni-Cr bifilar thermocoax resistance. An electric power of 45 W was necessary to reach a temperature of 790 K, measured with a chromel-alumel

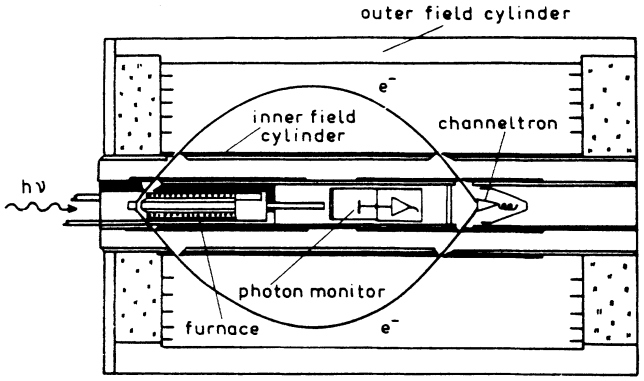

FIG. 3. Schematic view of the cylindrical mirror analyzer (CMA) and of the oven. The monochromatized beam of synchrotron radiation ($h\nu$) is focused into the source volume of the electron spectrometer. The oven is mounted on the axis of the CMA. The electrons are detected at the magic angle and counted with a channeltron (from Ref. 49).

TABLE I. Observed binding energies (eV) in the Ca^{1+*} $3p^6nl$ satellite spectrum and line assignments.

nl	Binding energy (eV) This work[a]	Optical[b]
$4s$	6.11	6.113
$3d$	7.83	7.810
$4p$	9.28	9.255
$5s$	12.60	12.581
$4d$	13.19	13.161
$5p$	13.64	13.625
$4f$	14.61	14.551
$5d$	15.15	15.130
$5f$	15.85	15.787
$5g$		15.804
$6d$	16.11	16.097
$7d$	16.70	16.644
Ca^{+2}		17.984

[a]Accuracy ±0.04 eV for $nl \leq 5p$, ±0.06 eV for $nl > 5p$.
[b]From Sugar and Corliss, Ref. 48.

thermocouple. At this temperature, the density of Ca atoms in the source volume of the analyzer was about 10^{12} atoms/cm^3. The metallic vapor was trapped on the surface of a water-cooled chamber after its interaction with the photons.

A slow time variation of the vapor density in the source volume was observed and was monitored by repeating, at regular time intervals, previously measured photoelectron spectra at a particular photon energy. The variation of the intensity of a photoelectron peak is then, once corrected for the decreasing photon flux, directly proportional to the variation of the density of Ca atoms during that period of time. In this way, it has been possible to correct for the relative variation of the density for the spectra recorded in the 40—120-eV photon-energy range. The accuracy of this correction is estimated to be about 8%.

B. Energy-level determination

The change of contact potential due to gradual deposit of target metal on the slits of the CMA influences the energy calibration of the analyzer. Known kinetic energies of Auger or autoionizing transitions can be used to establish the kinetic energy scale. For Ca, the Auger lines B' at 16.33 and 16.67 eV kinetic energy were used. The photon energy was then determined through measurement of the position of a photoelectron peak of known binding energy (lines B at 34.31 and 34.66 eV, or line Ca^+ $3p^64s\,^2S_{1/2}$ at 6.11-eV binding energy).[48] With this method, an accuracy of 0.01—0.02 eV is possible to reach when needed.

The absolute energy scale provided by the monochromator scale does not give the same level of accuracy. However, the *relative* variation in the photon energy could be accurately deduced from the change in the last digits of the monochromator scale while continuously scanning, in the *same* direction, a photon-energy region.

Using this procedure, we have measured the binding energies for the satellites corresponding to $3p^6nl$ and to $3p^5nln'l'$ excited states of Ca^+ ions. They are given in Tables I and II, respectively. The assignments for the $3p^6nl$ ionic states were straightforward using the previous analysis of Sugar and Corliss.[48] The assignments for the $3p^5nln'l'$ ionic states are more tentative in some cases, especially for the series of A satellites. In addition to the previous data of Mansfield and coworkers,[7,8] we had to consider the energy dependence of the partial cross sections in order to propose an identification. This will be discussed in Sec. VI. Moreover, the binding energy of the $3s$ electrons has been measured in this work for the first time, and is also given in Table II.

The results of our measurements for the energies of the Auger lines are given in Table III. They are compared with previous measurements by electron impact.[10] The overall agreement is excellent. Some of the lines in Table

TABLE II. Observed binding energies of the Ca^{1+*} $3s^23p^5nln'l'$ and $3s^13p^64s^2$ ionic states (from PE data).

Line	Binding energy (eV)	Assignment[b]
A_2	31.68 (±0.08)	$3p^53d4s\,^2P_{1/2,3/2}$
A_3	32.65 (±0.08)	$3p^53d4s(^3F)^2F_{5/2,7/2}$
A_4	33.24 (±0.06)	
A_5	33.82 (±0.06)	$3p^53d4s\,^4D_{1/2,3/2}$
B	34.312[a]	$3p^54s^2\,^2P_{3/2}$
	34.656[a]	$3p^54s^2\,^2P_{1/2}$
C	36.27 (±0.08)	$3p^5(3d^2\,^1S_0)^2P_{1/2,3/2}$
D	37.13 (±0.10)	
	37.51 (±0.10)	
E	39.60 (±0.10)	$3p^54s4p$[c]
F	42.64 (±0.08)	$3p^54s5s$[d]
$3s$	53.10 (±0.08)	$3s3p^64s^2\,^2S_{1/2}$

[a]From Sugar and Corliss, Ref. 48.
[b]From Mansfield and Ottley, Ref. 8.
[c]Tentative assignment from this work.
[d]From Walter and Schirmer, Ref. 19.

TABLE III. Observed energies of the Auger lines measured in this work. Lines 14 and 15 served as calibration lines for the other parts of the spectrum. Note that the assignment is uniquely given in terms of the *initial* state, the final state always being $3p^6(^1S)$. The assignment therefore coincides with that of the photoelectron lines.

Line number	Energy (eV) This work[a]	Ref. 10(b)	Ref. 10(a)[b]	Assignment[c]
1	13.01	13.00		$3p^5 3d4s\ ^4P_{1/2}$
2	13.55	13.49		$3p^5 3d4s(^3P)^2P_{1/2}$
3	13.63	13.60		$3p^5 3d4s\ ^2P_{3/2}$
4	13.92	13.87		
5	14.05	14.065		$3p^5 3d4s\ ^4F_{7/2}$
6	14.14	14.15		$3p^5 3d4s\ ^4F_{5/2}$
7	14.56	14.51		$3p^5 3d4s(^3F)^2F_{7/2}$
8	14.68	14.65		$3p^5 3d4s(^3F)^2F_{5/2}$
9	14.80	14.78		
10	14.92	14.99		
11	15.06	15.08		
12	15.15	15.17	15.19	
13	15.71	15.69		$3p^5 3d4s\ ^4D_{3/2}$
		15.79	15.75	$3p^5 3d4s\ ^4D_{1/2}$
14	16.33	16.329	16.35	$3p^5 4s^2\ ^2P_{3/2}$
15	16.64	16.675	16.69	$3p^5 4s^2\ ^2P_{1/2}$
16	17.55	17.515		
		17.565		
17	18.14	18.13	18.15	$3p^5(3d^2\ ^1S_0)\ ^2P_{3/2}$
18	18.41	18.40	18.41	$3p^5(3d^2\ ^1S_0)^2P_{1/2}$
19	18.53	18.525		
20	18.78	18.735		
		18.82		
21	19.23	19.27		
22	19.77	19.755		
		19.79		
23	20.07	20.08		
24	21.45	21.47		
25	21.81	21.82	21.83	$3p^5 4s4p$ [d]
26	22.33	22.30	22.29	
27	23.11	23.10		
28	23.59	23.59		
		23.62		
29	24.49	24.45		
30	24.79	24.75		$3p^5 4s5s$ [e]
31	35.04			$3s3p^6 4s^2\ ^2S_{1/2}$

[a]Accuracy ±0.04 eV.
[b]Accuracy ±0.06 eV.
[c]From Mansfield and Ottley, Ref. 8.
[d]Tentative assignment from this work.
[e]From Walter and Schirmer, Ref. 19.

III are measured here for the first time under photon impact because they can be seen only in the immediate vicinity of their threshold, under conditions of resonance and threshold excitation. In Figs. 1 and 2 one can observe a number of these lines. The assignment of the states was made with the help of the analysis of Mansfield and Ottley.[8] However, since any excited Ca^{1+} ion can be regarded as an ionization threshold, the energy dependence of the intensity of some of the lines was a crucial point to confirm the nature of the states involved. We shall return to this point when we discuss the partial cross sections.

One can also note, in Table III, that one Auger line corresponding to the decay of the $3s$ hole has been measured, also for the first time.

C. Intensity data analysis

Once corrected for the transmission of the CMA, for the variation of the density of Ca atoms, and for the variation of the flux of photons diffracted in the order considered, the integrated area under a photoelectron line is directly proportional to the cross section of the corre-

sponding transition.

The transmission of an electron spectrometer is known to be critically dependent on the kinetic energy of the electrons in the low-energy region. Recording the variation, with electron kinetic energy E, of the intensity of a photoelectron peak produced by the photoionization of a rare gas in a subshell of known photoionization cross section (Ne $2p^6$, Ar $3p^6$),[50,51] we have determined the transmission of the CMA for electron kinetic energies lower than 10 eV. The accuracy of this correction is estimated to be about 15%. For higher electron kinetic energies, we have checked that the transmission is proportional to E (Ref. 52).

There are no absolute photoabsorption data available in the energy range we have explored. Thus, to obtain absolute photoionization cross sections, our experimental data points for the $3p$ cross section σ_{3p} shown in Fig. 4 were normalized to our local-density random-phase approximation (LDRPA) calculation (solid line) of σ_{3p} using a least-squares fit. The experimental points represent the sum of the intensities of the main lines plus the satellite lines, assuming a constant fraction of 20% satellites over the entire energy range 40—120 eV (see Sec. VI). The error bars on the experimental points include the statistical error, as well as the uncertainties from variations of vapor density and photon flux. This leads to a relative error of about 15% on our experimental cross sections. The relative error is smaller, about 5%, on the branching ratios.

Note, finally, that in some photon-energy ranges cross-section data are missing because of the overlap between photoelectron and Auger lines.

III. RESONANCES AND DECAY CHANNELS

As a preparation for interpreting partial photoionization cross sections, in this section we shall give a schematic description of the excitation and decay of various resonances in atomic Ca. We shall analyze a model spectrum (Fig. 5) and discuss the basic characteristics of the branching of resonances into a few important decay channels.

The absorption spectrum of Ca vapor in the $3p$ resonance region has been extensively studied with high resolution by Mansfield and Newsom,[7] who also classified a large number of levels with the help of LS-dependent Hartree-Fock calculations. We shall use that work as a reference. In addition, we refer to the recent measurement of Ca^{1+} and Ca^{2+} cross sections by Sato *et al.*[12]

In Fig. 5 we show a *schematic* picture of the $3p$ resonance excitations and of the photoionization continua of atomic Ca.

In the *photoabsorption* spectrum, corresponding to the sum of all photoionization channels, the continuum normalized $3p^5 4s^2 nl$ resonances smoothly join the $3p^5 4s^2 \epsilon l$ continuum; there is no jump at the principal $3p$ threshold.

However, when we look at the *emission* channels, the picture is quite different. The discrete $3p^5 4s^2 nl$ excitations lie below the principal $3p$ threshold and consequently *must decay* into the $3p^6 4s \epsilon l_\epsilon$ and $3p^6 n'l' \epsilon l_\epsilon$ channels (the sum of which represents the Ca^{1+} channel), and into the $3p^5 4s 3d \epsilon l_\epsilon$ channels (which mainly contribute to the Ca^{2+} channel due to subsequent Auger decay). In other words, the total oscillator strength of the discrete region must show up in these channels. However, when we cross the $3p^5 4s^2$ thresholds, the emission goes almost entirely into the $3p^5 4s^2 \epsilon l_\epsilon$ channel (i.e., the principal Ca^{2+} final-state channel). The cross section of the other channels therefore *must rapidly drop* across the $3p$ principal threshold.

The transfer of strength between the channels is connected with the fact that the Auger line is formed already below threshold in the quasicontinuum as a resonant band of highly excited PE satellite lines.[5] When the photon energy is increased, the resonance leaves these channels, crosses the double-ionization threshold, and appears as a true Auger line. As a result, there will be a rapid increase of the Ca^{2+} yield and decrease of the Ca^{1+} yield.

In the absence of $3p^{-1}$ shakedown satellites, the sum of the Ca^{1+} channels would have dropped from an average value of about 35—40 Mb just below the $3p$ threshold down to about 1 Mb just above threshold.[53] This would have led to a huge Ca^{2+}- to Ca^{1+}-yield ratio (≈ 40). In reality, as we shall see, the $3p^5 4s 3d \epsilon l_\epsilon$ and $3p^5 3d^2 \epsilon l_\epsilon$

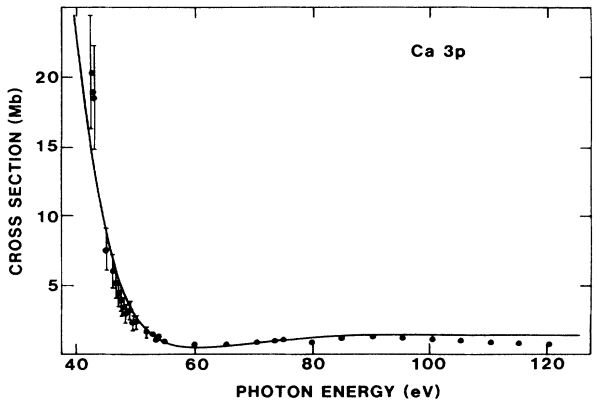

FIG. 4. Experimental and theoretical data for the $3p$ cross section used for the normalization procedure of all cross sections measured in this work. At high photon energy, the size of the error bars is within the surface of the points.

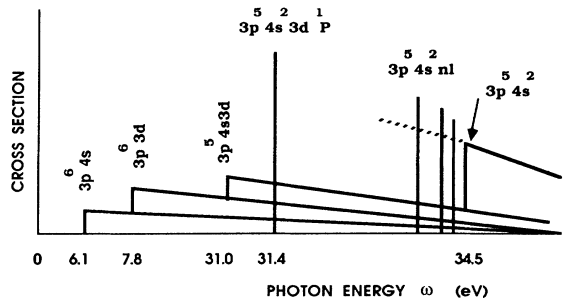

FIG. 5. Schematic picture of ionization continua and resonances in calcium.

shakedown channels (and thus the Ca^{2+} channel) pick up considerable strength and therefore strongly reduce the jump at the main $3p$ threshold.

We shall now give a more detailed description of a number of important and typical cases (see also Ref. 1 for an introduction and Ref. 2 for further details). In the $3p$ resonance region we have the following general scheme for excitation and decay:

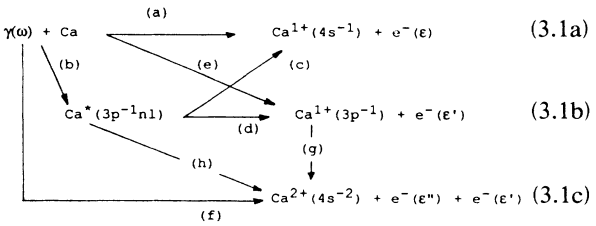

(3.1a)

(3.1b)

(3.1c)

In (3.1) only primary configurations have been marked; the possibility of $4s \rightarrow 3d$ and $4s^2 \rightarrow 3d^2$ reorganization, leading to satellite levels in both excitation and emission, is understood. The different paths in (3.1) have the following meanings (ν labels the $i \rightarrow \epsilon$ channel):

(a) Direct $4s$ single ionization; excitation amplitude $t^{\nu}_{0\epsilon}$.

(b) Resonant (r) $3p$ excitation; excitation dipole matrix element d_r, resonance frequency (excitation energy) ω_r, and decay width Γ_r.

(c) and (d) Decay channels (ν) of the resonant $3p$ excitation; decay matrix elements $V^{\nu}_{\epsilon r}$; partial decay widths $\Gamma^{\nu}_r = 2\pi |V^{\nu}_{\epsilon r}|^2$. Path (d) may lead to $3p^{-1}$ shakedown satellites; e.g., $3p^{-1}4s^{-1}3d$.

(e) Direct $3p$ single ionization; excitation amplitude $t^{\nu}_{0\epsilon}$.

(f) Direct $4s$ double ionization.

(g) Two-step double ionization via $3p^{-1}$ Auger decay.

(h) Decay of the resonant $3p$ excitation via direct $4s$ double ionization.

$t^{\nu}_{0\epsilon}$, d_r, and $V^{\nu}_{\epsilon r}$ are complex and frequency dependent, and ω_r and Γ_r are real and frequency dependent. The photoionization amplitude in channel ν may then be written as[2,5] (ω is the photon energy)

$$t^{\nu}_{\epsilon}(\omega) = t^{\nu}_{0\epsilon} - \frac{V^{\nu}_{\epsilon r} d_r}{\omega_r - i\Gamma_r/2 - \omega} \tag{3.2}$$

and the partial (channel) photoionization cross section is given by

$$\sigma^{\nu}_{\epsilon}(\omega) \sim |t^{\nu}_{\epsilon}(\omega)|^2 \tag{3.3a}$$

$$\sim |\langle \epsilon | r(\omega) | i \rangle|^2 \tag{3.3b}$$

$$= |\langle \epsilon | r\epsilon^{-1}(r;\omega) | i \rangle|^2 \tag{3.3c}$$

$$\approx \sigma^{\nu}_{0\epsilon}(\omega) / |\epsilon_{\nu}(\omega)|^2 . \tag{3.3d}$$

In Eq. (3.3b) the many-electron effects (polarization) have been put into an effective dipole operator (effective driving field),[2,3] which is expressed in terms of a space- and frequency-dependent dielectric response function in Eq. (3.3c). Finally, in Eq. (3.3d) we have expressed the channel cross section in terms of the direct channel cross section $\sigma^{\nu}_{0\epsilon}(\omega)$ modified by a channel-dependent dielectric function $\epsilon_{\nu}(\omega)$, which contains the resonance effects.

The energy-resolved photoelectron spectrum in each channel (PE line) has the form

$$d\sigma^{\nu}_{\epsilon}/d\epsilon = \sigma^{\nu}_{\epsilon}(\omega)\delta(\epsilon - \epsilon^{\nu} - \omega) , \tag{3.4}$$

where we have taken the final state (ϵ^{ν}) to be sharp. This is an approximation for the $3p^{-1}$ PE lines (which, however, are not true final states due to subsequent Auger decay).

The total photoionization (essentially photoabsorption) cross section is given by

$$\sigma(\omega) = \sum_{\nu} \int d\epsilon \, d\sigma^{\nu}_{\epsilon}/d\epsilon \tag{3.5a}$$

$$= \sum_{\nu} \sigma^{\nu}(\omega) . \tag{3.5b}$$

In the vicinity of a reasonably symmetry resonance one may neglect the direct term,[54] in which case Eqs. (3.2) and (3.3) give the photoionization cross section in each channel,

$$\sigma^{\nu}(\omega) \sim |d_r|^2 \frac{\Gamma_r/2\pi}{(\omega - \omega_r)^2 + (\Gamma_r/2)^2} \frac{\Gamma^{\nu}_r}{\Gamma_r} . \tag{3.6}$$

The total photoionization (photoabsorption) cross section in the region close to a resonance is finally given by

$$\sigma(\omega) \sim |d_r|^2 \frac{\Gamma_r/2\pi}{(\omega - \omega_r)^2 + (\Gamma_r/2)^2} , \tag{3.7}$$

where

$$\Gamma_r = \sum_{\nu} \Gamma^{\nu}_r . \tag{3.8}$$

For a given series of $3p^{-1}nl$ resonances (r) and a given continuum channel (ν), the continuum-normalized coupling strength (coupling density; roughly Γ^{ν}_r divided by the distance between resonances) will remain roughly constant. However, when one passes a threshold and a new channel opens up, the total decay width Γ_r will increase. In Eq. (3.6), the branching ratio Γ^{ν}_r/Γ_r will therefore decrease with increasing photon energy as one proceeds through the $3p^{-1}nl$ resonances and more and more $3p^{-1}$ thresholds open up. This represents conservation of probability and is the major reason for the attenuation of the progression of $3p^{-1}nl$ resonances in the $Ca^{1+}(3p^6n'l')$ channels, i.e., the $4s^{-1}$ main line and satellites (present work), as well as the ion yield (Ref. 12).

We shall now describe a number of important and typical cases which will frequently occur in our discussions of the experimental results in Secs. IV—VI. Some of these points have already been discussed in some detail in Ref. 2.

A. The $3p^5 4s^2 3d\ ^1P$ "giant dipole resonance" at 31.41 eV

This resonance is the most intense discrete excitation in Ca. Although it is a single-electron excitation it has to be

described using many-electron methods which taken into account the large polarizability of the $3p$ shell;[2,43] one may talk about collective behavior.

Figure 5 gives a schematic picture of the final-state continua (channels) to which the $3p^5 4s^2 3d\ ^1P$ giant dipole resonance can decay. We then have the following excitation and decay scheme:

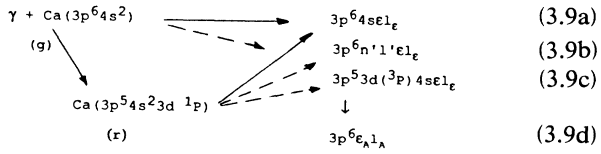

In (3.9) the solid long arrows indicate the major excitation and decay channels, dashed arrows indicate weaker channels.

The photon-energy variation of some of the $4s^{-1}$ channels is shown in Fig. 6 (from Ref. 1). From this variation we have measured the energies of a number of resonances. These energies are given in Table IV, with the indication of which ionization channels are enhanced in each case. For most of the resonances there is good agreement with the photoabsorption measurements of Mansfield and Newsom.[7]

The *major decay channel* is via $3p$-$3d$ *recombination* leading to emission of a $4s$ electron [$(r)\rightarrow(a)$ in (3.9), autoionization; actually, $(r)\rightarrow(g)\rightarrow(a)$ might be an even better description]. Due to the large $3p$-$3d$ overlap, this decay process is about ten times faster than the $3p$-Auger decay $3p^5 4s^2 \rightarrow 3p^6 \epsilon l_\epsilon$ which lies behind the $(r)\rightarrow(b)$ decay process in (3.9) and which leads to $4s$ satellites.

In fact, resonance excitation of the *satellites* also seems to proceed mainly via $3p$-$3d$ recombination back to the ground state followed by emission in the $3p^6 n'l'$ satellite channel $(r)\rightarrow(g)\rightarrow(b)$. This is indicated by the present experimental results (Sec. V), which show that the $4s$ satellite-to-main-line branching ratios are approximately constant, keeping their off-resonance values, when one sweeps across the $3p^5 4s^2 3d\ ^1P$ resonance. This suggests that at least the low-lying satellites are directly excited from the ground state by ground-state correlation (e.g., $3p^6 3d$, $3p^6 4p$) or shakeup (e.g., $3p^6 5s$), and that the resonant enhancement occurs via the mean field [Eq. (3.3b)].

There is also an interesting decay to a quasistationary "final" Ca^{1+} state with a $3p$-$3d$ triplet-coupled electron-hole pair (3.9c). The direct decay $(r)\rightarrow(c)$ (dashed line) represents an exchange-driven[5,55] spin-flip decay process. However, according to the above discussion, decays which do not pass via the ground state should be weak. At present, we therefore believe more in the indirect decay mechanism $(r)\rightarrow(g)\rightarrow(c)$. This could be interpreted as enhancement of the $(g)\rightarrow(c)$ shakedown $3p^5 3d(^3P)4s\epsilon l_\epsilon$ transition due to the resonating mean field [Eq. (3.3b)]. The excitation curve for this and similar $3p^{-1}$ satellites cannot be studied directly with the present experimental setup since they appear at very low kinetic energies. However, the desired satellite excitation curves are identical to the excitation curves for the corresponding *Auger satellite* lines (3.9d). Examples and further discussion will be given in Sec. VI.

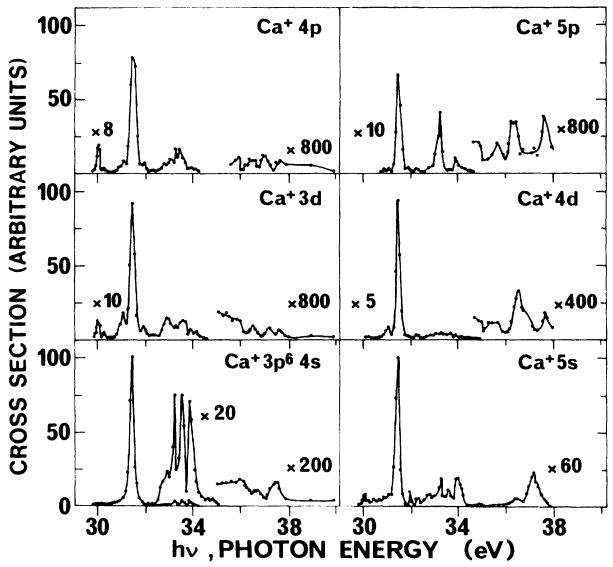

FIG. 6. Relative cross sections of the main ($4s$) exit channel and five satellite ($3d$,$4p$,$5s$,$4d$,$5p$) $3p^6 nl$ exit channels for the photoionization of atomic calcium. The width of most of the resonant structures is mainly governed by the bandpass of the monochromator. For this reason, and because of possible variations of the density in the photon-energy region above 36 eV, no absolute scale is indicated for the cross section (1 Mb would correspond, in principle, to 0.3 arbitrary units; this conversion factor is valid for all figures presented in this paper).

B. Higher d-channel single-excitation resonances, $3p^5 4snd$, $n \geq 4$

A schematic excitation and decay scheme is given by

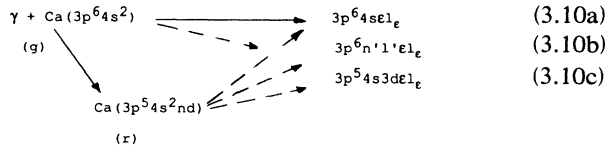

For the $3p^5 4s^2 nd\ ^1P$ transitions, the $3p^{-1}\rightarrow 4s^{-2}$ Auger interaction $V^A_{\epsilon r}$ is constant while the $nd\rightarrow 3p$ recombination (autoionization) interaction $V^a_{\epsilon r}$ decreases with increasing n. For $n=3$ the recombination dominates, as discussed above. For $n=4$ the radial extent of the $4s$ and $4d$ orbitals are comparable; the direct decay rates to (3.10a) and (3.10b) are therefore comparable, leading to comparable resonance enhancements of the $4s^{-1}$ main line and a number of $4s^{-1}$ satellites. This is also clear from the experimental results in Fig. 6 around 33.0–33.5 eV.

For $n \geq 5$ the $nd\rightarrow 3p$ recombination rate will be lower than the Auger rate, and the resonance intensity should branch more and more towards the satellite spectrum with increasing n. This is, in fact, what happens in Fig. 6.

TABLE IV. Energies of the major resonances observed from the enhanced intensity of photoelectron lines in some ionization channels. Our results are compared with the photoabsorption data of Mansfield and Newsom (Ref. 7).

These measurements		Photoabsorption measurements[b]	
Energy[a] (eV)	Main enhanced continuum channel Ca^+3p^5nl	Energy (eV)	Assignment
27.80	$3d$	27.79	$3p^5(3d^2\,^1D)(^2P)4s\,^1P_1$
29.98	$4p,4d,3d,5p,4s$	29.98	$3p^5(3d^3\,^3P_1)\,^3P_1$
30.16	$4s,4p,3d$	30.15	$3p^54s4p^2\,^5P_1$
		30.19	$3p^5(4p^2\,^1S)(^2P)3d\,^3P_1$
		30.21	$3p^5(4p^2\,^3P)(^2P)3d\,^3D_1$
30.88	$4s,3d,4d,4p$	30.83	$3p^5(3d^3\,^2P)^3D_1$
		30.85	$3p^5(3d^2\,^1S)(^2P)4s\,^3P_1$
31.08	$4s,3d,4d,4p$	31.01	$3p^5(3d^3\,^4P)^3P_1$
31.45	$4s,4d,3d,4p,5d,5p$	31.41	$3p^54s^2\,^2P_{1/2}3d\,^1P_1$ (series c)
31.60	$4s,4p,4d,5d,3d$	31.58	$3p^5(3d^2\,^1S)(^2P)4s\,^1P_1$
		31.62	$3p^54s^24d\,^3P_1$
31.92	$4s,4p,3d,4d$	31.96	$3p^54s^2\,^2P_{3/2}5s$ (series b)
32.27	$4d,5p,4p,3d$	32.26	$3p^54s^2\,^2P_{1/2}5s$ (series d)
32.78	$3d,4s,4p,4d,5d$	32.76	$3p^5(4p^2\,^1D)(^2D)4s\,^3D_1$
32.94	$3d,4s,6d,5d,4p,4d$	32.95	
33.09	$4p,5p,3d,4s,4d$	33.16	$3p^54s^2\,^2P_{3/2}6s$ (series b)
33.26	$4s,5p,6p,4p$	33.22	$3p^54s^2\,^2P_{3/2}4d$ (series a)
		33.24	$3p^5(4p^2\,^1S)3d\,^3D_1$
33.60	$4s,3d,4p,4d$	33.56	$3p^54s^2\,^2P_{1/2}4d\,^1P_1$ (series c)
		33.59	$3p^54s^2\,^2P_{3/2}5d$ (series a)
		33.63	$3p^54s^2\,^2P_{3/2}7s$ (series b)
33.88	$6d,4s,6p,5p$	33.86	$3p^54s^2\,^2P_{3/2}6d$ (series a)
34.10	$4s,3d,5p,4p$	33.97—34.21	$3p^54s^2\,^2P_{3/2}nd$ $n=7$—12 (series a)
		33.98	$3p^54s^2\,^2P_{1/2}5d$ (series c)
35.63	$4s,4d,5p,3d$	35.63	$3p^5(3d^3\,^1S_0)(^2P_{3/2})6d$ (series e)
35.98	$4s,5s$		
36.39	$5s,4s,4d,5p$	36.26	$3p^5(3d^3\,^4P)^3P_1$
36.56	$4s,4d,5s$	36.48	$3p^5(3d^2\,^3P)(^2P)4s\,^3P_1$
37.12	$5s,6s$	37.09	$3p^5(3d^3\,^2P)^1P_1$
37.64	$4s,5s,6s,4d,5p$	37.79	$3p^5(4p^2\,^3P)3d\,^1P_1$
38.01	$6s,4s,5p,4d$		

[a]Accuracy ±0.08 eV.
[b]From Mansfield and Newson, Ref. 7.

Without this branching towards the satellites, the $4s^{-1}$ main-line cross section would reach much higher values in the resonances.

C. The s-channel single-electron excitation resonances $3p^54s^2ns$

This case is characterized by the fact that $ns\rightarrow 3p$ recombination is always much slower than $3p^{-1}$ Auger decay. The excitation and decay scheme is given by

$$\gamma + Ca(3p^64s^2)\ (g) \longrightarrow \begin{cases} 3p^64s\varepsilon l_\varepsilon & (3.11a) \\ 3p^6n'l'\varepsilon l_\varepsilon & (3.11b) \\ 3p^54s3d\varepsilon l_\varepsilon & (3.11c) \end{cases}$$

$$Ca(3p^54s^2ns)\ (r)$$

and the resonance mainly branches to the $4s^{-1}$ (3.11b) and $3p^{-1}$ (3.11c) satellite spectra. This will be further discussed in Secs. IV A, V, and VI.

D. Triple-electron excitations

This case concerns a number of resonances in the 30—38-eV region. An important group of levels is lying in the vicinity of the $3p$-$3d\,^1P$ (giant dipole) resonance and probably derive much of their intensity from interaction with the giant resonance (Fig. 6).

A particularly nice example is the isolated resonance at 30.0 eV.[1,2] It has been classified[7] as $Ca[3p^5(3d^3\,^2P)^3P_1]$. However, such a resonance must be strongly affected by correlation effects. A more general way of describing it would be in terms of configuration interaction, e.g., $3p^53d(3d^2+4p^2+5s^2+\ldots)$.[1,2] This should also be a

general description of any triply excited resonance in the neighborhood of the $3p$-$3d\ ^1P$ giant dipole resonance at 31.41 eV.

The excitation and decay scheme is then given by

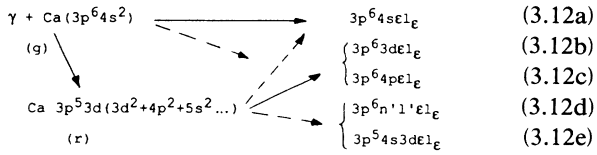

(3.12a)
(3.12b)
(3.12c)
(3.12d)
(3.12e)

This case has been discussed fairly extensively in Refs. 1 and 2 in connection with the 30.0-eV resonance. Qualitatively speaking, the decay is characterized by $3p$-$3d$ recombination with emission of a $3d$, $4p$, or $5s$ electron, etc. This leaves the system almost exclusively in an *excited ionic state;* emission of a $4s$ electron (ionic ground state) is a weaker higher-order effect, involving, e.g., final-state correlation and shakedown,[2] and the resonance can hardly be seen (Fig. 6).

Finally, note that the $3p^5 4s 3d\epsilon l_\epsilon$ continuum is not available to the 30.0-eV resonance (begins at 31.0 eV). Otherwise, these types of channels are fairly important.

E. The $3p^5 3d(^1P)4s5s$ double-excitation resonance

The strongest $3p^{-1}$ satellite (*F,F'* in Fig. 2) may be associated with a $4s$-$5s$ shakeup transition, about 8 eV above the principal $3p^{-1}$ lines. One could then expect to find some trace of this transition also as a satellite to the $3p$-$3d\ ^1P$ resonance transition (it should be rather weak since the $3p \rightarrow 3d$ excitation is quite localized and will be much less of a perturbation than the $3p^{-1}$ hole).

The $4s$-$5s$ excitation energy in the *ground state* should be around 5 eV [$5s$ binding energy is approximately 2 eV with a $3p$ hole (Tables II and IV); $4s$ binding energy 6.11 eV (Table I)]. Since the $3p^5 3d(^1P)$ excitation energy is 31.4 eV, the $3p^5 3d(^1P)4s5s$ satellite excitation energy should then lie around 37 eV.

If the resonance exists, its excitation and decay scheme would typically be

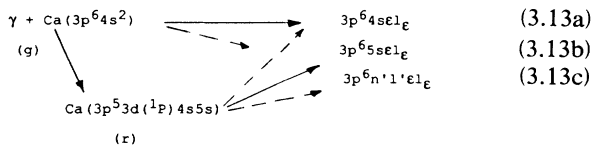

(3.13a)
(3.13b)
(3.13c)

i.e., $3p \rightarrow 3d$ recombination should predominantly ionize the remaining $4s$ electron, leaving the ion in an excited state corresponding to the $4s^{-2}5s$ satellite.

A violently resonating $4s^{-2}5s$ satellite has, in fact, been observed at 37.15 eV (Fig. 6); (see also Fig. 3 in Ref. 1). Moreover, the entire 36–38-eV region shows prominent resonance structure, as is evident in Fig. 6 (see also Fig. 1).

It should be noted that, according to Mansfield and Newsom,[7] there are a number of other types of double and triple excitations in the 36–38-eV region [cf. Eq. (3.12)]. These are no doubt responsible for much of the observed structure. However, it is difficult to understand how the result could be a very strongly resonating $4s^{-2}5s$ satellite.

F. Multiple-excitation resonances such as $3p^5(3d^2)nl$, $3p^5(4s3d)nl$, $3p^5(4s4p)nl$, $3p^5(4p^2)nl$, and $3p^5(4s5s)nl$

In view of the complicated $3p^{-1}$ satellite structure there must be a large number of multiply excited resonances such as $3p^5(3d^2)nl$, $3p^5(4s3d)nl$, $3p^5(4s4p)nl$, $3p^5(4p^2)nl$, and $3p^5(4s5s)nl$. We have already discussed cases such as $3p^5(3d^2)3d$, $3p^5(4p^2)3d$, and $3p^5(4s5s)3d$ above. Except for the case that $nl = 3d$ (where possible), the ionic core ($3p$ satellite) will in most cases decay (to the "double-ionization" continuum $3p^6\epsilon l_\epsilon$) on the same time scale as, or more rapidly than, recombination transitions involving the nl electron. The situation is then similar to what has been discussed in Secs. III B and III C, namely, that the decay is spread over many channels, more or less heavily weighted towards the $3p^6 n'l'$ satellites.

IV. $4s$-, $3p$-, AND $3s$-SUBSHELL CROSS SECTIONS

In this section we shall present results for the variation of the intensities of the main PE lines in the 26—120-eV photon-energy range. In what concerns the experimental data, the absolute cross-section scale (in Mb) has been established by fitting the experimentally determined $3p$ subshell cross section between 40 and 120 eV to the result of an LDRPA calculation for the $3p$ photoionization cross section, as has been described in Sec. II and shown in Fig. 4. In all of the figures presenting cross sections the arbitrary-unit (a.u.) scale is the same, with the conversion factor 1 a.u. $\sim$ 3 Mb.

From the cross sections of the main lines we shall get an overall view of the dynamics of atomic Ca, and we shall discover various resonance and threshold regions, including regions that have not been studied before. We emphasize that in the resonance regions both main lines and satellites must be considered together in order to have a complete picture of the physics of the excitation and decay processes, i.e., the dynamics.

A. $4s$-main line PE cross section

The experimental $4s$ main-line cross section is shown in Fig. 7, covering the $3p$-resonance region, and in Fig. 8, covering the continuum extending up to 120-eV photon energy. In Fig. 7 the dominating resonant feature is the $3p^5 4s^2 3d\ ^1P$ giant dipole resonance at 31.41 eV, which mainly decays to the $3p^6 4s\epsilon p$ channel. More precisely, the branching ratios are the same off and on resonance (this will be demonstrated experimentally in Sec. V). This is connected with the fact that the $3p^5 4s^2 3d\ ^1P$ resonance can be described in terms of a resonance in the local effective electric field and therefore affects all ionization channels essentially in the same way.

A closer inspection of the $3p^5 4s^2 3d\ ^1P$ resonance reveals structure at 31.4—31.5 eV photon energy.[7] According to Mansfield and Newsom[7] the structure is due mainly to triple ($3p^5 3d^3$) excitations, with some contribution

from double ($3p^5 3d 4p^2$) excitations. Normally, one would expect triple excitations to show up only very weakly in the $3p^6 4s\epsilon p$ single-electron ionization channel (cf. Sec. III D). However, the closeness of the multiple excitations to the $3p^5 4s^2 3d\ ^1P$ resonance leads to strong configuration interaction; the oscillator strength of the $3p^5 4s^2 3d\ ^1P$ resonance simply becomes distributed over a number of levels, which decay to the $3p^6 4s\epsilon p$ single-electron ionization channel in proportion to their content of the driving $3p^5 4s^2 3d\ ^1P$ giant dipole resonance. However, we note that the resonance-level structure is more evident in the Ca^{1+}, and in particular the Ca^{2+}, -ion spectra of Sato *et al.*[12] The reason is that the ion spectra include the contributions from highly excited satellites and from the double-ionization continuum, which are more selectively excited from the multiple-excitation structures. This will emerge very clearly from the cross sections of $4s^{-1}$ and $3p^{-1}$ satellites, to be presented and discussed in Secs. V and VI.

The $3p^5 4s^2 3d\ ^1P$ giant dipole resonance has an asymmetric Fano profile, and there is a broad but pronounced interference minimum in the $4s$ cross section around 32.2 eV. The interference comes from the competition between the direct and resonant channels in Eq. (3.7a), which leads to a photoionization amplitude of the form shown in Eq. (3.2). The direct term may not be neglected if we want to describe the resonance over an extended photon-energy region. The resonance-line profile has been calculated by Altun and Kelly[15] giving good qualitative agreement with experiment.[1,2,56] The natural width of the resonance is primarily due to autoionization [Eq. (3.9a)] and is of the order of the photon bandpass used to scan the resonance (≈ 0.1 eV).

The higher $3p^5 4s^2 nd$ single excitations (except perhaps $n=4$) show up rather weakly in the $4s$ main-line cross section; the resonances in this region branch in a fairly democratic manner onto most of the possible ionic final states (Sec. III B).

Furthermore, we note a few particular things: there is no sign of any $3p^5 4s^2 5s$ resonances around 32 eV (Sec. III C); the structure just below 33 eV is due to triple excitations; as discussed in Sec. III, the cross section rapidly drops to a very low value when one crosses the main $3p$ thresholds just above 34 eV.

There is very interesting structure in the 36—38-eV region. Part of this structure is probably due to the $3p^5 3d(^1P)4s5s$ double excitation (see Secs. III E and V). The pronounced structures in the $4s$ cross section around 36 eV and around 38 eV seem to be correlated with the thresholds of $3p$ satellites. The structures might then be interpreted as rapid drops of the $4s$ cross section when new $3p$ ionization channels open up.

Figure 8 shows the experimental $4s$ PE cross section above the main $3p$ thresholds, together with the theoretical results of LDRPA and relativistic random-phase approximation (RRPA) calculations. The main impression

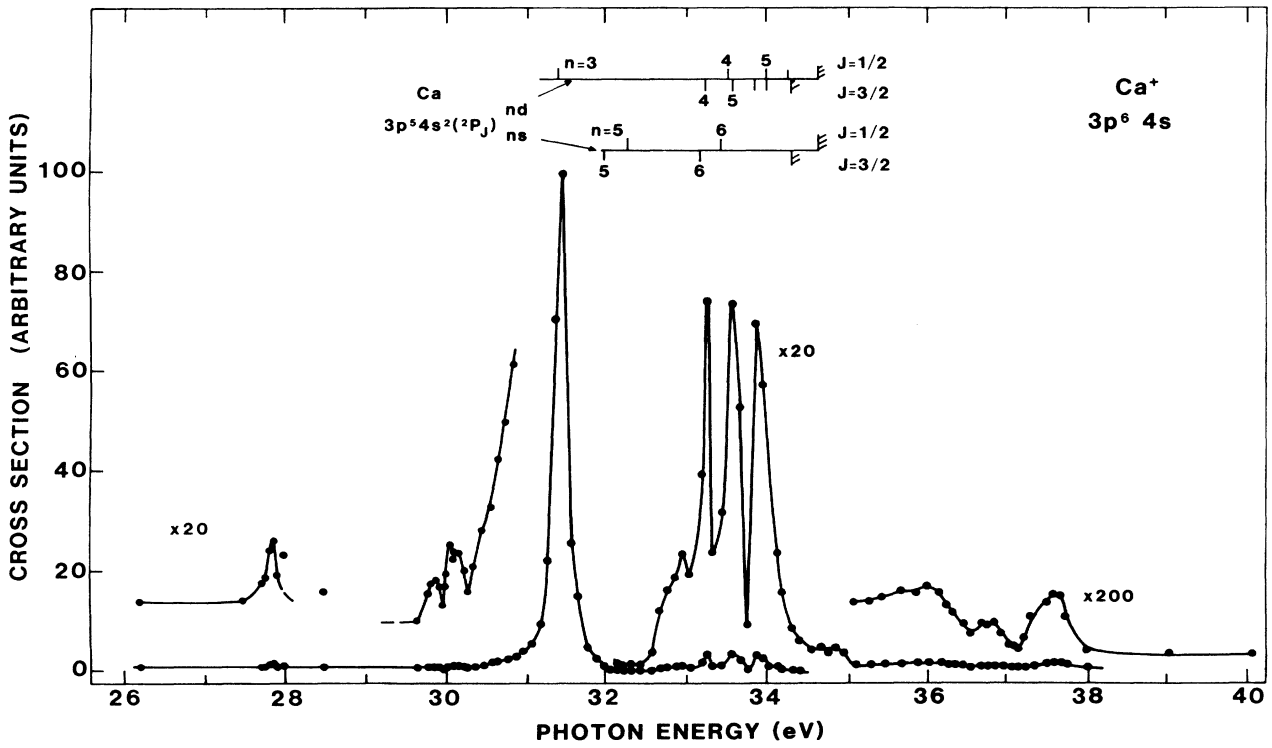

FIG. 7. Variation of the $4s$ photoionization cross section in the $3p$-resonance region. The energy positions of the main $3p^5 4s^2 ns$ and $3p^5 4s^2 nd$ excitations, taken from the photoabsorption work of Mansfield and Newsom,[7] are marked in the figure. The cross-section scale is the same as in Fig. 6.

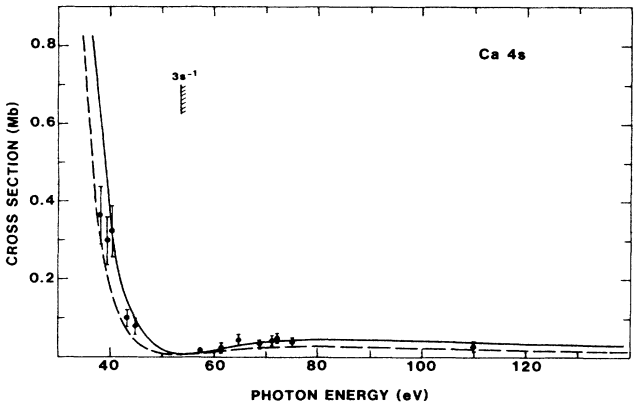

FIG. 8. Variation of the $4s$ photoionization cross section as a function of the photon energy. ●: present work. Theoretical curves are the result of our LDRPA calculation (——) and of a RRPA calculation by Desmukh and Johnson (Ref. 14).

is that of a smooth continuum without any pronounced resonances. Moreover, there is good qualitative agreement between experiment and theory. The experimental values of the $4s$ cross section are given in Table V.

Regarding the difference between the LDRPA and the RRPA results in Fig. 8, it should be mentioned that in the present LDRPA calculation the coupling between the subshells on the average is a little too strong, including only mean-field interaction (bubble diagrams, dipole-dipole interaction, electron-hole exchange). In the RRPA the subshell interaction also includes a contribution from electron-hole scattering (ladder diagrams), which reduces the coupling strength somewhat. In Fig. 8 we would therefore expect that the RRPA results could be more accurate than those of the LDRPA. [Note that the nonrelativistic random-phase approximation with exchange (RPAE) (Ref. 13) closely agrees with the RRPA for Ca.]

Finally note in Fig. 8 that one expects resonance structure around 40 eV (double excitations, $3p^{-1}$ satellite thresholds) and that there are clear indications of resonance structure around 70 eV photon energy (double excitations, $3p^{-2}$ thresholds). This will become more evident in the $3p$ main-line and satellite cross sections (see Fig. 9 and Sec. VI).

TABLE V. $4s$ and $3s$ main-line photoionization cross sections. The absolute scale has been fixed by fitting the experimental $3p$ cross section to the calculated LDRPA cross section in Fig. 4. Accuracy on the photon energy is ±0.08 eV. $\Delta\sigma/\sigma \simeq 20\%$.

$h\nu$ (eV)	σ_{4s} (Mb)	σ_{3s} (Mb)
38.01	0.365	
39.04	0.301	
40.06	0.323	
43.03	0.099	
44.54	0.079	
57.12	0.018	
61.57	0.024	
64.48	0.043	
68.89	0.031	
70.98	0.042	
72.07	0.049	
74.86	0.038	
75.20		0.170
80.00		0.058
85.12		0.112
90.50		0.105
95.49		0.136
100.61		0.122
105.53		0.101
110.30	0.027	
110.59		0.113
115.51		0.092
120.50	0.056	0.151

B. $3p$ subshell cross sections

The $3p$ main PE lines become experimentally accessible about 3 eV above threshold (limitation imposed by the low-energy transmission of the photoelectron analyzer) and can be accurately measured from about 40 eV. However, in the photon-energy region extending from threshold to 40 eV, the intensity of Auger lines is representative of the $3p$ cross section, because of the mirror symmetry between the Auger spectrum and the photoelectron spectrum (cf. Fig. 2). This has been quantitatively checked in the photon-energy regions where both spectra were clearly distinguishable without overlapping parts. Thus, below 40 eV, the variation of the $3p$ cross section is accurately obtained by summing up the intensity of the Auger lines. A proper normalization of the cross section in the two photon-energy ranges was made at 40 eV.

The $3p$ *main-line* cross section in the 40—120-eV range is given in Table VI (the normalization procedure was described in Sec. II). Figure 9 shows the $3p$ main-line cross section scaled up by 25%, representing an *estimated* total $3p$ cross section (20% coming from $3p$ satellites). The *total (subshell)* $3p$ cross section between 34 and 40 eV is shown in Fig. 10 (includes explicitly all channels involving $3p$ satellites).

The normalization of the $3p$ main-line cross section is a serious problem because of the intensity of $3p$ satellites, the observed part of which amounts to about 20% at $h\nu = 120$ eV (see Sec. VI). Since the theoretical cross sections (LDRPA, RRPA) do not take account of the $3p^{-1}$ core-hole spectrum, they provide *subshell* cross sections corresponding to the *sum of the main line and all of the shakeup satellites* (also the shakeoff continua).

From an *experimental* point of view, the simplest way would, of course, be to normalize the experimental $3p^{-1}$ *main-line cross section* over a wide photon-energy range to a good theoretical calculation of the same quantity. However, a reliable calculation of this kind is not possible at present; it would have to take into account frequency-dependent relaxation effects in the neighborhood of ionization thresholds. This method of normalization therefore does not work because of limitations of present theory.

A closely related approach would be to normalize according to the above procedure, in a range of photon ener-

TABLE VI. $3p$ main-line photoionization cross section. The absolute scale has been fixed by fitting to the calculated LDRPA cross section in Fig. 4. Accuracy on the photon energy is ±0.08 eV. $\Delta\sigma_{3p}/\sigma_{3p} \simeq 15\%$.

$h\nu$ (eV)	σ_{3p} (Mb)	$h\nu$ (eV)	σ_{3p} (Mb)
42.32	16.25	72.18	0.76
42.36	16.32	72.32	0.76
42.56	15.17	72.50	0.76
42.68	14.86	72.70	0.74
42.81	14.86	72.90	0.82
45.01	6.01	73.08	0.82
46.04	4.78	73.34	0.96
46.52	4.10	73.50	0.94
46.99	3.50	73.70	0.84
47.47	3.14	73.86	0.75
48.02	2.73	74.14	0.85
48.53	2.37	74.26	1.04
49.03	2.51	74.44	0.79
49.62	1.82	74.64	1.00
50.12	1.84	75.00	0.89
52.01	1.23	75.20	0.79
53.04	1.14	75.32	0.89
53.57	0.92	75.46	0.83
54.00	0.96	80.00	0.68
54.99	0.75	85.12	0.93
60.04	0.53	90.50	1.01
65.48	0.56	95.49	1.01
70.16	0.85	100.61	0.88
70.58	0.82	105.53	0.76
70.90	0.68	105.59	0.69
71.04	0.79	115.51	0.63
71.36	0.72	120.50	0.55
71.74	0.77		
72.00	0.76		

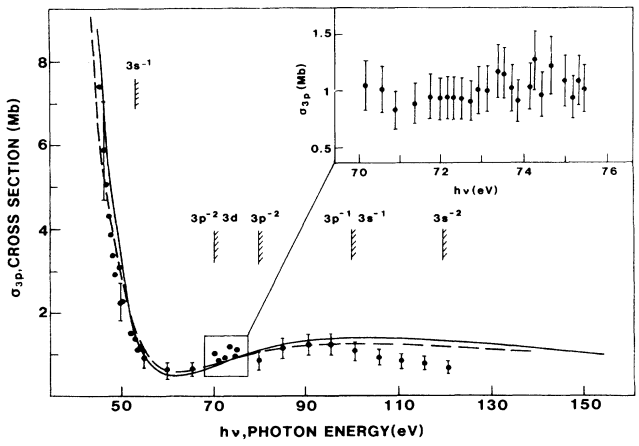

FIG. 9. Variation of the $3p$ photoionization cross section as a function of the photon energy. ●: present work ($3p$ main-line cross section scaled up by 25% to include the estimated satellite intensity). The theoretical results are from the same calculations as in Fig. 8. The inset shows, on a magnified scale, the variation of the cross section in the energy region of double excitations in the $3p$ shell.

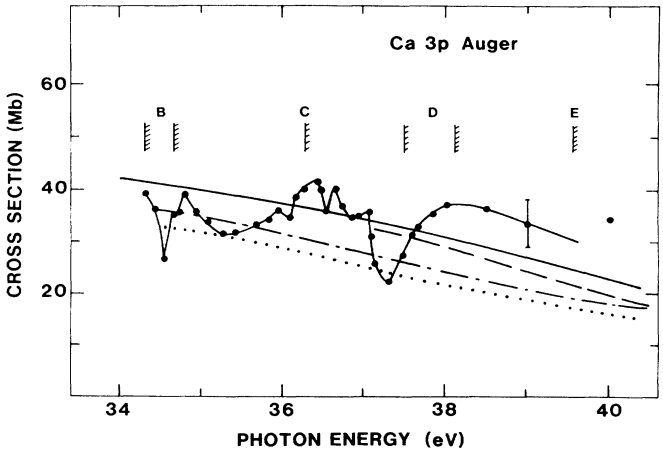

FIG. 10. Variation of the $3p$ photoionization cross section as a function of the photon energy in the resonance region of $3p$ multiple excitations. The experimental values have been obtained from the intensity of the Auger lines—the solid line joining the points only serves to guide the eye. The ionization thresholds corresponding to various excited states of $3p$-core ionized Ca ions are marked in the figure as measured in this work (see Table II and Figs. 1 and 2). Theoretical results are from different calculations: LDRPA (——, this work), RRPA (Ref. 14) (— — —), MBPT (Ref. 15) (· · ·, length; —·—·—·, velocity). The LDA $3p$ threshold lies around 28 eV. Between 28 and 34.3 eV the LDRPA represents an average of the discrete oscillator strength.

gies sufficiently high above the satellite thresholds that satellite-to-main-line branching ratios have become *constant*, i.e., independent of the photon energy. In this (sudden) limit the $3p$-main-line—to $3p$-subshell—cross-section ratio can be accurately estimated theoretically[4] (ratio $\approx |\langle 3p^{-1}; \text{frozen} \,|\, 3p^{-1}; \text{relaxed}\rangle|^2$, where $|3p^{-1}\rangle$ represents the many-electron wave function with a $3p$ hole).

This latter scheme, however, does not work because of a combination of physical and experimental reasons. Even at 120 eV photon energy, which was the highest value chosen experimentally, we seem to be in the region of shakeup satellite thresholds, i.e., far from the sudden limit. In Fig. 9 the deviation between experiment and theory is very clear above 90 eV. The theoretical calculations agree quite well between themselves, and are sufficiently well understood that we may rule out errors in the calculations. The simplest explanation for the deviation is that there is still some important dynamics going on.

In Fig. 9 we have marked thresholds for $3p$ and $3s$ double excitations (rough estimate, configuration average). The deviations between theory and experiment seems to occur in the region of double excitations in the $3p$ and $3s$ subshells. This then suggests that the experimental points should coincide again with the calculated curves at some elevated photon energies, perhaps in the range above 150 eV, where a proper normalization could be made.

In the sudden limit, the frozen-core RPA type of cross

sections strictly correspond to subshell cross sections. From a theoretical point of view, one would therefore like to compare the $3p$-subshell cross section with the experimental results for the sum of $3p$ main lines, discrete satellites, and satellite continuum at high photon energies. This is, however, not realistic because of the low $3p$ cross section and the low flux of synchrotron radiation available at present.

By going to low photon energies there is a realistic chance experimentally to measure the intensities of the $3p^{-1}$ satellites and to add them to the $3p^{-1}$ main lines to obtain subshell cross sections (such results will be given in Sec. VI; the summation was actually done in the case of the $3p^{-1}$ Auger lines, which forms the basis for the $3p$-subshell cross section in Fig. 10). Moreover, experience shows that RPA type of calculations (if necessary, with relaxed-core potential) give good average agreement with photoabsorption cross sections also in threshold regions. This means that the most realistic scheme in the end will be to normalize in the low-to-intermediate energy region by comparing, in principle, subshell cross sections.

In the present case, the experimental $3p$ *main-line* cross section has been *scaled up by 25%,* incorporating an average of the *experimentally measured* relative $3p$ satellite intensity over a wide photon-energy region (Sec. VI). The resulting $3p$-subshell cross section has then been normalized to the theoretical LDRPA $3p$ subshell cross section, by fitting over an extended region (40—120 eV), as shown in Figs. 4 and 9.

The 20% relative $3p$-satellite intensity is consistent with the theoretical *high-energy* result by Walter and Schirmer[19] which suggests that the theoretical $3p$-subshell cross section should be scaled down by 18% in order to give the $3p$ main-line cross section. As we shall see later in Sec. VI, the relative intensities of the strongest $3p$ satellites C, E, and F are together around 20% all the way down to 40 eV (the relative strength of all satellites between 35—40 eV amounts to as much as 30—35 %). This means that the relative $3p$ satellite strength is very large down in the vicinity of the $3p$ thresholds, and the simple scaling procedure therefore works reasonably well.

In Fig. 10 the experimental $3p$-subshell cross section shows pronounced resonance structure, corresponding to double or triple excitations. The most prominent resonance is a very strong window resonance at $h\nu=37.15$ eV (cf. Sec. III E). The sum of all the other partial cross sections (satellites) does not seem to fill up this hole, which suggests that this window resonance should be observed in the *absorption* spectrum. The experimental absorption spectrum (Mansfield and Newsom[7]) indeed shows broad peaks and broad dip in the correct energy range, but the intensities of these features are difficult to judge due to lack of linearity of the photographic plate. There is, however, a marked similarity. The photoion data of Sato *et al.*[12] unfortunately cut off a little too early, at about 36 eV.

Figure 11, finally, shows our experimental results for the $3p_{3/2}$-$3p_{1/2}$ main-line branching ratio, also obtained from the relative intensity of the main Auger lines. Above 50 eV photon energy, on the average the ratio follows fairly well the RRPA prediction, which is quite close

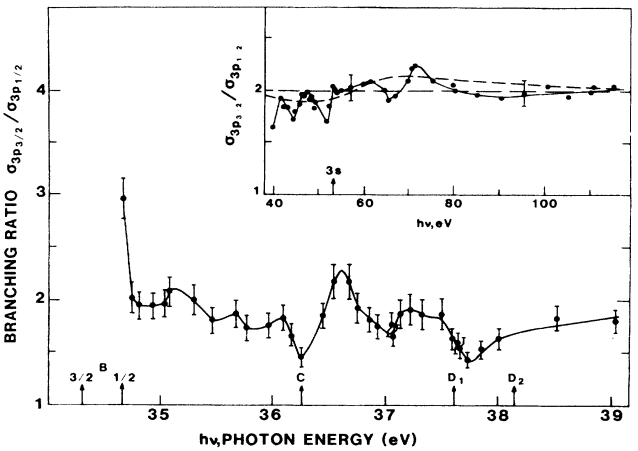

FIG. 11. Variation of the $\sigma(3p^5 4s^2\,{}^2P_{3/2})/\sigma(3p^5 4s^2\,{}^2P_{1/2})$ branching ratio in the region of $3p$ thresholds and above (inset). ●: present work. The inset shows two theoretical curves: the statistical branching ratio (=2), and the result of an RRPA calculation by Desmukh and Johnson (Ref. 14).

to the statistical ratio of 2. On the other hand, the deviations are so strong, in particular in the region from threshold to 50 eV, that a comparison with the RRPA is not particularly meaningful. A realistic calculation of the branching ratio clearly must include the $3p$-satellite structure and associated resonances.

In Fig. 11 we have marked the $3p^{-1}$ and $3s^{-1}$ main lines and the $3p^{-1}$ satellite thresholds (Table II), and other relevant thresholds are given in Fig. 9. The results suggest a strong correlation between extended regions of thresholds and resonances (e.g., 36—53 eV, 65—110 eV) and pronounced deviations from the RRPA result. Moreover, there is a suggested detailed correlation between dips in the ratio and positions of thresholds in the 36—53-eV region.

Finally, there is pronounced variation at the position of the window resonance just above 37 eV.

Qualitatively, it is easy to find reasons for the variations of the branching ratio, in terms of intensity sharing between a main line and its satellites, including interaction between the associated ionization channels. When the photon energy is increased to above a satellite threshold there will be a reduction of the main-line cross section. The $3p^{-1}$ satellite structures C,E,F show a spin-orbit splitting similar to the $3p^{-1}$ main line (cf. Fig. 2); the satellite associated with the $3p_{3/2}$ main line will emerge before the $3p_{1/2}$ satellite, and as a consequence there will be a dip in the $3p_{3/2}$-$3p_{1/2}$ main-line branching ratio.

C. The 3*s* main-line PE cross section

The intensity variation of the $3s^{-1}$ main PE line is shown in Fig. 12, together with theoretical results of LDRPA (present work) and RRPA (RPAE) (Ref. 14) calculations for the $3s$ subshell ionization cross section. The normalization of the experimental $3s^{-1}$ cross section has

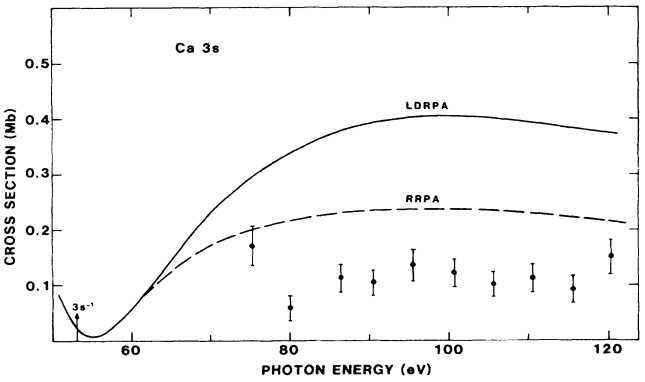

FIG. 12. Variation of the $3s$ photoionization cross section (main line) of atomic calcium as a function of the photon energy. ●: experimental results, this work; —— LDRPA (calculation, this work); — — —, RRPA (Ref. 14).

been determined independently, via the experimental $3s/3p$ main-line branching ratio and the $3p$ normalization.

The experimental values of the $3s$ main-line cross section are given in Table V.

To the experimental $3s^{-1}$ main-line cross section in Fig. 12 (Table V) one should add the cross sections of all the $3s^{-1}$ satellites. This total $3s^{-1}$ cross section should then be compared with the theoretical $3s$ (subshell) cross sections in Fig. 12. In the present experiment, it is impossible to identify and sum the $3s^{-1}$ satellites due to low intensities and overlapping spectra, and due to lack of angular information to sort out the ^2S satellites (cf. Ref. 57). We therefore have no independent experimental estimate of the relative $3s^{-1}$-satellite intensity.

Theoretically, the $3s^{-1}$ cross section is very difficult to describe in a proper manner.[57–60] The $3s$-$3p$ shell coupling provided by the RRPA (RPAE)[13,14] is essential but far from sufficient. The Dirac-Fock (Hartree-Fock) $3s$ threshold in Ca lies at 61.5 eV (Ref. 14), i.e., about 8.5 eV above the experimental $3s$ threshold at 53.1 eV (Table II). Of these 8.5 eV, about 2.5 eV represents the monopole relaxation shift, while 5.5 eV is due to dipole relaxation (virtual giant-Coster-Kronig process) and correlation (i.e., CI in the final and initial states).[4,19] The threshold lowering is associated with intensity sharing with satellites mainly of the type $3p^{-2}3d,4d,\ldots,\epsilon d$ (Walter and Schirmer,[19] Wendin[4]). In this respect the problem is analogous to the case of Ar,[57–60] and also to the cases of Xe (Refs. 4, 60 and 61) and Ba.[4]

According to Walter and Schirmer,[19] the $3s$ main line represents 0.65 of the total $3s$ strength (only a small part of this loss of strength is due to monopole shakeup). Scaling the RRPA cross section in Fig. 12 by 0.65 brings it into very good agreement with experiment in the 80–120 photon-energy region. The experimental data points happen to fall in a region with double excitations and double-excitation thresholds, which probably explains the irregular variation of the cross section (cf. the $3p$ cross section in Fig. 9).

The LDA $3s^{-1}$ threshold at 46 eV is much too low (due to self-interaction effects).[62] However, this has the advantage that the interference minimum in the $3s^{-1}$ cross section stands out clearly. The result suggests that there is in reality a minimum in the continuum just above the $3s^{-1}$ main threshold, which makes it difficult to observe the $3s^{-1}$ main line close to threshold. An analogous cross-section minimum due to interchannel coupling exists in Ar, but at kinetic energies well above (≈ 15 eV) threshold (see, e.g., Refs. 13 and 59). The RRPA (RPAE) is then capable of describing the region of the minimum and works quite well down to the Dirac-(Hartree-) Fock threshold.[13]

The difference between the LDRPA and RRPA (RPAE) $3s$ cross sections in Fig. 12 is probably due to the fact that the present LDRPA calculation exaggerates the strength of the intershell coupling (as discussed in connection with the $4s$ cross section). Similar results have been found by Parpia, Johnson, and Radojević[63] in the case of the $5s$ cross section in Xe using the linearized time-dependent local-density approximation (TDLDA, similar to the LDRPA).

V. 4s PE SATELLITE CROSS SECTIONS

A PE-AE spectrum with prominent $4s$ satellites has already been shown in Fig. 1, and the detailed variation of the intensity of the $4s$ main PE line has been given in Figs. 7.

In this section we shall present equally detailed cross sections for a number of $4s$ satellites, $3p^63d$, $4p$, $5s$, $4d$, and $5p$, as well as satellite—to—main-line ($4s$) branching ratios. An overview of these spectra has already been given by Bizau *et al.*[1] and Wendin.[2]

The $4s$ main-line cross section in Fig. 7 is dominated by *single*-electron excitations. However, in the satellite cross sections in Figs. 13–21, apart from the $3p^54s^23d\ ^1P$ resonance at 31.41 eV, the resonance structure is largely dominated by *triple* (and perhaps double) excitations (cf. Mansfield and Newsom[7]). The region from 33.2 eV ($3p^54s^24d$) to threshold should in principle be dominated by single-electron excitations, heavily mixed with double and triple excitations. However, with the present photon bandpass in that region (0.1 eV), we have no possibility of resolving the structure (except the $n=4$ resonance: see, e.g., Fig. 7), and we therefore observe only *"large-scale"* variations of intensities and branching ratios.

To be able to describe the relative strengths of the $4s^{-1}$ (and $3p^{-1}$) main line and satellites represents a very sensitive test of our understanding of the character of the resonances and of the couplings. These problems are connected with structural details and therefore require detailed calculations. However, these are *important details,* well worth a careful examination, since they require good *qualitative* descriptions of correlation effects in the initial and final states. We have touched upon this problem in Sec. III, and we shall meet it many times in the presentation of experimental data.

A. The $3p^63d$ cross section (Figs. 13 and 14)

Let us discuss in some detail the characteristics of the intensity variation of the $3p^63d$ satellite.

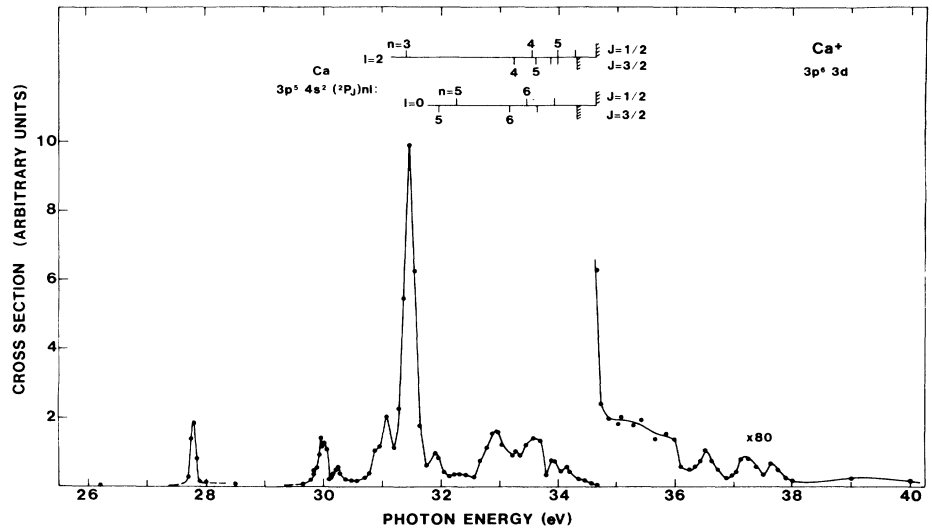

FIG. 13. Variation of the photoionization cross section for production of the $3p^6 3d$ excited state of Ca^{1+} ions. In this figure, as in Fig. 7 and Figs. 14–21, the energy positions of the $3p^5 4s^2 ns$ and $3p^5 4s^2 nd$ excitations are taken from Mansfield and Newsom,[7] and the cross-section scale is given only in arbitrary units.

In Fig. 13 the dominant peak at 31.41 eV is due to the $3p^5 4s^2 3d\ ^1P$ single-electron excitation. This is, in fact, the only *single*-electron excitation that can be clearly seen; *all other peaks refer to triple (in some cases possibly double) excitations.* This becomes particularly clear in Fig. 14, showing the branching ratio $R(3d/4s)$. Three things should first be noticed in Fig. 14.

(i) There is no structure in the branching ratio at the $3p^5 4s^2 3d\ ^1P$ resonance at 31.4 eV.

(ii) The huge peak around 32.2 eV is due to the interference minimum in the $4s$ cross section.

(iii) Most of the pronounced structure in the branching ratio seems to originate from triple excitations $3p^5 3d^3$ [from comparison with Mansfield and Newsom,[7] in accordance with the theoretical considerations in Sec. III].

We would like to emphasize that the branching-ratio curve must be used with great care and always together with the individual partial cross sections. *The branching-ratio curve cannot be interpreted on its own* (the same may often be said about angular distributions).

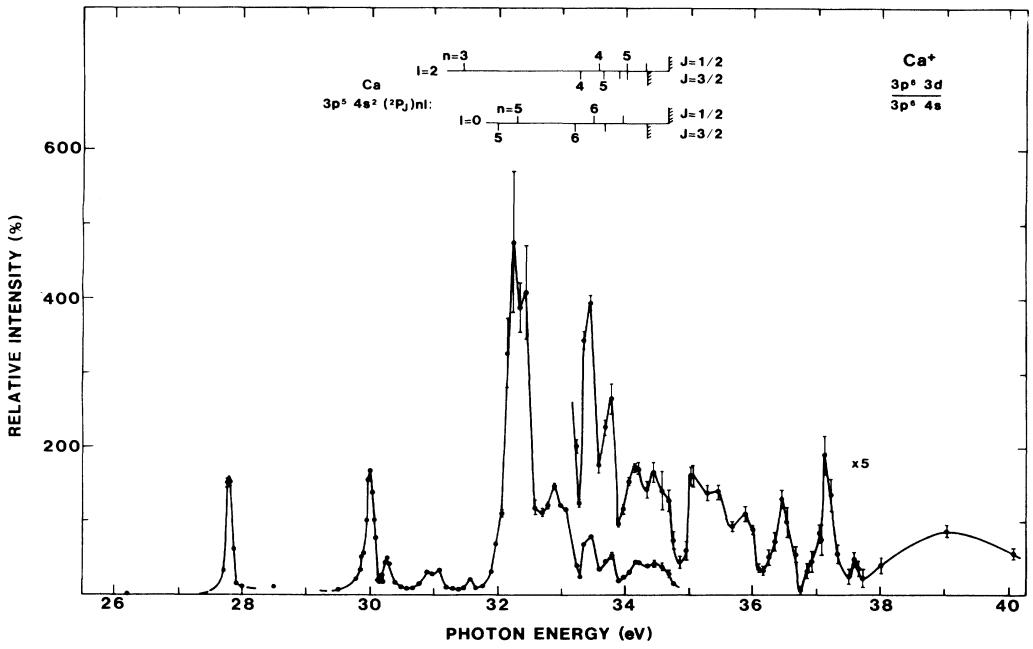

FIG. 14. Variation of the branching ratio between the $3p^6 3d$ PE satellite and the main $3p^6 4s$ line.

The whole frequency range from zero to well above the $3p$ threshold is dominated by the polarization of the $3p$ shell (effective field). We can therefore not talk about any region outside the influence of the $3p \rightarrow 3d$ resonance.

Having noted this, we may nevertheless distinguish between off- and on-resonance situations, off-resonance representing flat portions of the continuum. "Broad" off-resonance regions occur around 29 eV photon energy (Figs. 7 and 13), where $R(3d/4s) \approx 6\%$ (Fig. 14). Moreover, in the resonance-free region around 30.5 eV this ratio is $\approx 9\%$ (Fig. 14). These ratios should essentially correspond to generation of the $3d$ satellite via $4s^2 \rightarrow 3d^2$ ground-state correlation combined with photoemission of one of the $3d$ electrons [$3p$ ionization combined with inelastic scattering ($4s \rightarrow 3d$) might also contribute]. Note, however, that in the off-resonance 26—27-eV region the ratio appears to be very small, ≈ 0. Moreover, in the off-resonance region at 21.2 eV (He I excitation[6]) the ratio is approximately 4.5%.

At and around the $3p^5 4s^2 3d\ ^1P$ giant dipole resonance, the ratio $R(3d/4s)$ essentially keeps the same constant value, $\approx 8\%$. This may be understood in terms of the effective local field (3.3b), which is common to the ionization channels, and in terms of approximately channel-independent dielectric functions (3.3d) which factor out and cancel in the branching ratio. The only structure in the ratio $R(3d/4s)$ in this region occurs at 31.6 eV, corresponding to the high-energy shoulder on the $3p^5 4s^2 3d\ ^1P$ resonance at 31.41 eV, due to triple excitations. This little bump in the ratio may look very tiny. *However,* it nevertheless represents a twofold increase of the $3d$ satellite relative to the $4s$ main line, which itself happens to be very prominent.

Due to the large variation of the branching ratio R with the character of the resonance (see Sec. III), this ratio is useful for discovering and identifying weak-resonance structures which mainly show up in the satellite (Ca^{1+*}) channels. For instance, it is difficult to resolve the resonance structure in the 32—34-eV region in Fig. 13. However, in the ratio in Fig. 14 the peaks clearly correspond to *triple excitations,* while the *single excitations appear at the minima* of the ratio.

We further note that all the peaks in the branching ratio in the 29.8—31.8-eV range correspond to triple excitations, which mainly decay to the satellite channels. Triple excitations hardly show up in the main $4s^{-1}$ channel, and may even give rise to a dip (window resonance, e.g., at 30.0 eV).

The resonance at 27.8 eV poses a bit of a problem. Mansfield and Newsom[7] have classified the resonance as $3p^5(3d^2\ ^1D)^2P4s\ ^1P$. In view of the strong $3p$-$3d$ exchange interaction, an alternative description could be $(3p^5 3d)^1P\, 3d\,(^2P)4s\ ^1P$, which suggests that the most likely decay would be $3d \rightarrow 3p$ recombination (dipole transition) together with ejection of the other $3d$ electron. Such a decay would leave the Ca^+ ion predominently in its ground state $3p^6 4s$, and would lead to a relatively low $3d$- to $4s$-intensity ratio.

However, this is not in accordance with the experimental result (Fig. 14) which shows a very pronounced and selective resonance enhancement of the $3p^6 3d$ satellite over the $3p^6 4s$ main line. Such behavior would be easier to associate with a classification $3p^5 4s^2 3d\ ^3D$, which has been associated[7] with a somewhat weaker resonance at 27.15 eV. For such a resonance the $3d \rightarrow 3p$ recombination rate would be very low and $3p^{-1} \rightarrow 4s^{-2}$ Auger decay should be the dominant decay mechanism, leaving a resonantly and selectively excited $4s^{-2}3d$ (i.e., $3p^6 3d$) ionic final-state configuration. Unfortunately, we have not investigated the behavior of the resonance at 27.15 eV and therefore cannot determine experimentally whether the two resonances behave in different or similar ways.

Finally, we note that the $3p^5 4s^2 5s$ resonances at 32.0 and 32.2 eV hardly show up in the $3d$ cross section. However, they do show up clearly in the ratio in Fig. 14 in the form of a pronounced shoulder and a dip in the

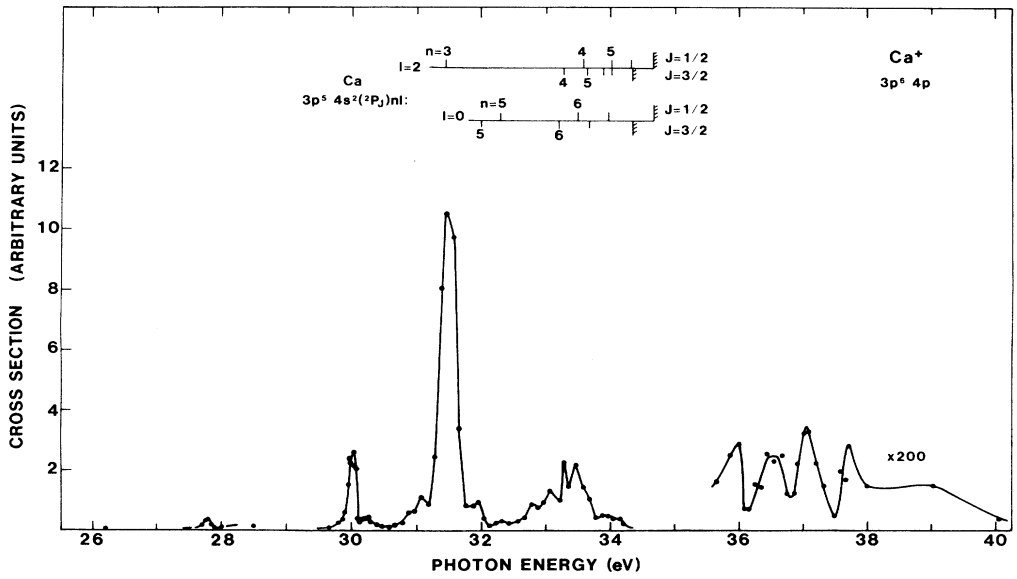

FIG. 15. Variation of the photoionization cross section for production of the $3p^6 4p$ excited state of Ca^{1+} ions.

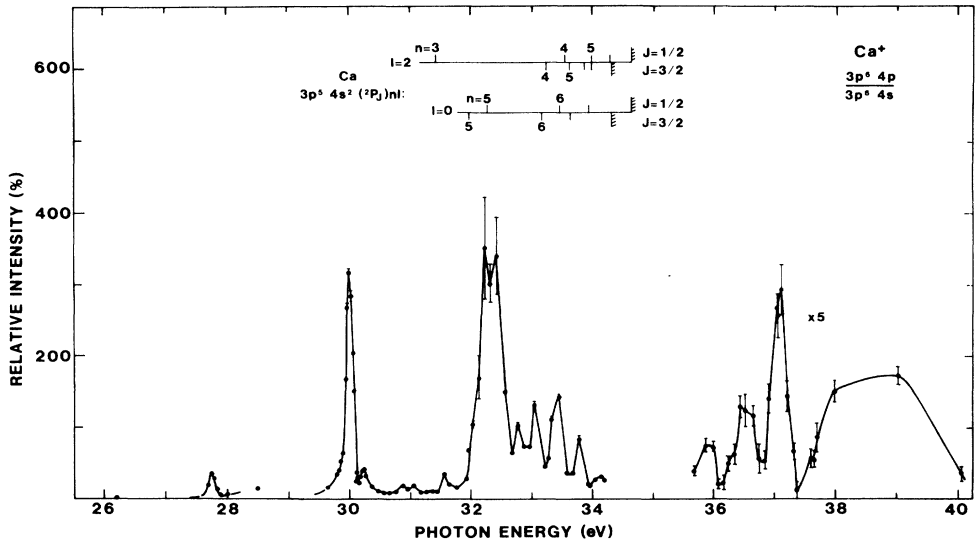

FIG. 16. Variation of the branching ratio between the $3p^6 4p$ PE satellite and the main $3p^6 4s$ line.

huge peak at the interference minimum of the $4s$ cross section. This confirms (Sec. III C) that such resonances recombine (autoionize) very slowly and therefore branch towards satellites through $3p$ Auger decay.

B. The $3p^6 4p$ cross section (Figs. 15 and 16)

The $3p^6 4p$ cross section in Fig. 15 shows many similarities to the $3d$ cross section. Most of the differences seem to be *quantitative,* concerning variations of branching ratios, of importance for comparison with detailed calculations. These variations can be very large, indeed, as in the case of the 27.8-eV resonance (factor of 5). Major differences (factors of 2) occur frequently, e.g., around 30 and 31 eV and in the 32.8—33.5-eV region.

We emphasize again that the variations reflect significant differences in correlation effects in the initial and intermediate states, and provide a sensitive test of theoretical models.

C. The $3p^6 5s$ cross section (Fig. 17 and 18)

Although the $3p^6 5s$ satellite is very weak off resonance, it shows quite a dramatic variation with photon energy which is highly significant for qualitative understanding of the dynamics of excitation and decay processes.

First of all we note from Fig. 18 that the $5s$- to $4s$-intensity ratio contains relatively little detailed structure. On the whole, the $3p^6 5s$ satellite therefore follows the behavior of the $4s$ parent line, a behavior that can be expected from a *monopole shakeup satellite;* The resonance profile of the $3p \rightarrow 3d$ giant dipole resonance in Fig. 17 is highly asymmetrical. In particular, there is an interference zero at 31.8 eV, leading to the zero value of the $5s$- to $4s$-intensity ratio in Fig. 18. This interference minimum (zero) occurs before the corresponding broad interference minimum in the $4s$ main line around 32.2 eV, the likely reason being that the direct transition is relatively weaker for the $3p^6 5s$ satellite.

We note that the $3p \rightarrow 5s$ resonances at 32.0 and 32.2 eV show up very clearly in Figs. 17 and 18. This points to the importance of selective excitation of the $5s$ satellite through decay of the $3p^5 4s^2 5s$ resonance via a $3p^{-1} \rightarrow 4s^{-2}$ Auger process (see Sec. III).

In Fig. 17 the broad peak around 34 eV represents a conglomerate of highly excited $3p^5 4s^2 nl$ levels, and the high-energy cutoff is due to the opening up of the main $3p$-ionization channels. In the $5s$- to $4s$-intensity ratio in Fig. 18 the narrow peak at 34.0 eV may possibly be associated with a $3p_{1/2} \rightarrow 5d$ resonance. If so, the $5s$ satellite excitation is selective in the sense that the excited electron is placed in the $n = 5$ main shell ($5d$) but there must also be an exchange of angular momentum with the "Auger" electron to cause scattering from $5d$ to $5s$.

Finally, a *unique* feature about the $5s$ cross section in Figs. 17 and 18 is the *huge* resonance peak at 37.15 eV (see also Fig. 3 in Ref. 1). As discussed in Sec. III E we tentatively interpret this peak in terms of a $3p^5 3d(^1P)4s\,5s$ double excitation, which preferentially decays to the Ca^{1+} $3p^6 5s$ final state.

D. The $3p^6 4d$ cross section (Figs. 19—21)

At first sight, looking at Figs. 19 and 20, one might think that the $4d$ cross section is rather similar to the $3d$ cross section (Sec. V A, Figs. 15 and 16). However, when one plots the $4d$- to $3d$-intensity ratio (Fig. 21), one immediately discovers *huge relative variations,* reflecting qualitative differences in the decay mechanisms.

The most obvious difference is that the $3p^5 4s^2 3d\ ^1P$ resonance at 31.41 eV is twice as strong as in the $3d$ case, while it should have been many times smaller if the $3p \rightarrow 3d$ recombination (effective driving-field) mecha-

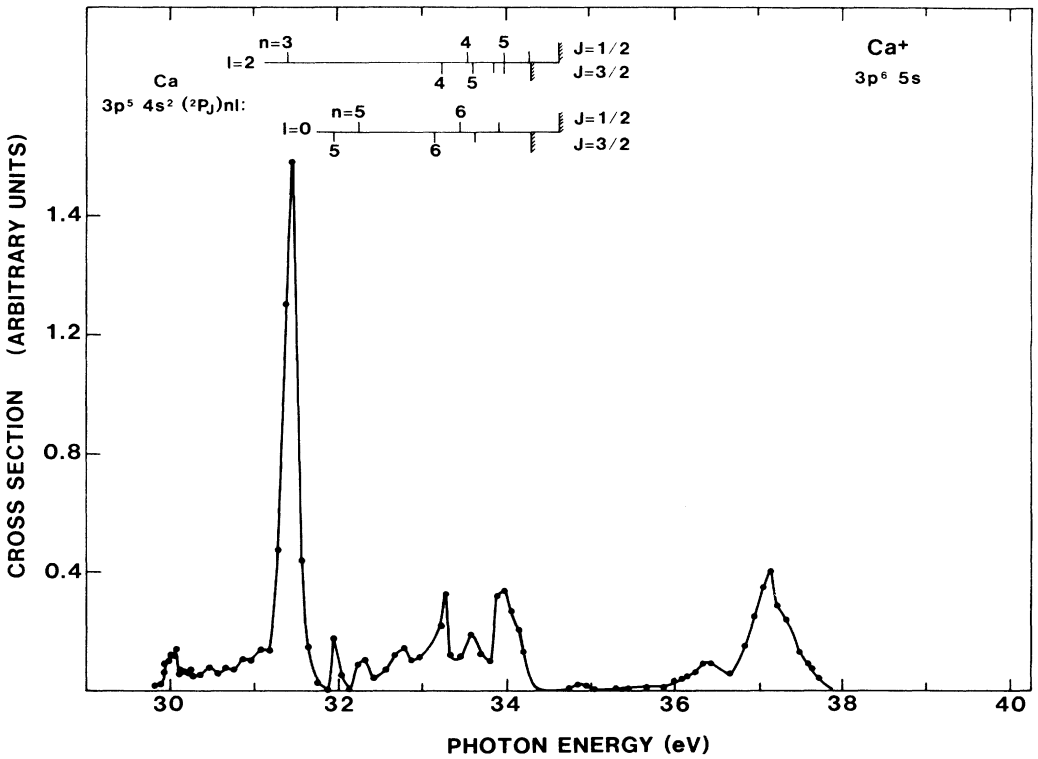

FIG. 17. Variation of the photoionization cross section for production of the $3p^6 5s$ excited state of Ca^{1+} ions.

nism were the only important one. This can be understood if there are also selective (resonant satellite) mechanisms.

In Fig. 20 the resonant behavior of the $4d$- to $4s$-intensity ratio around 31.41 eV may not look impressive, but nevertheless the variation relative to the off-resonance situation is quite large. This is reflected in the $4d$- to $3d$-intensity ratio in Fig. 21, where the $3p^5 4s^2 3d\ ^1P$ resonance

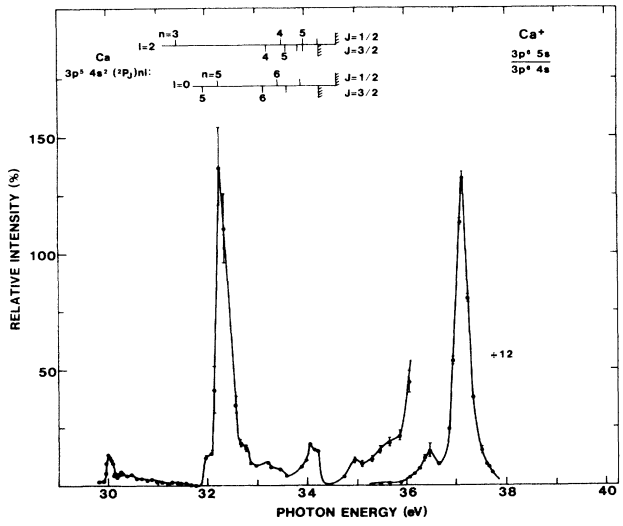

FIG. 18. Variation of the branching ratio between the $3p^6 5s$ PE satellite and the main $3p^6 4s$ line.

stands out clear. In fact, the level structure in the 30—32-eV region involving singly and triply excited levels is clearly resolved.

We also note that the structure in the region of the interference minimum around 32.2 eV emerges very clearly.

E. The $3p^6 5p$ cross section (Figs. 22 and 23)

Also the $3p^6 5p$ PE cross section is dominated by relatively few but prominent features, which suggests that a few special excitation and/or decay mechanisms play the important role.

For example, the two prominent and sharp resonances in the 33—34-eV region in Fig. 22 correlate with the positions of $3p^5 4s^2 4d$ and $3p^5 4s^2 6d$ resonances ($J=\frac{3}{2}$). However, the $5p$ satellite (like $4p$ or any other p satellite) cannot be reached via a single-electron $3p^5 4s^2 nl$ excitation followed by Auger decay *unless* one considers angular momentum transfer via (direct and/or exchange) scattering of the Auger p electron by the bound nl electron.

Other possible candidates for the resonant level might be a doubly excited $3p^5 4s 4p^2$ configuration (see Sec. III) and/or a triply excited $3p^5 3d 4p^2$ configuration, which should have preferred decay to Ca^{1+} $3p^6 n'p$ final states.

Finally, it seems that only the $3d$, $4p$, and $5s$ satellites behave such that the $3p^5 4s^2 3d\ ^1P$ resonance factors out of the satellite-to-main-line ratio, giving a low, constant ratio around 31.41 eV. If this is the case, the $5p$ and $4d$ satellites (and all the higher ones) are really resonantly enhanced relative to the $4s$ main line, e.g., via Auger decay of the intermediate resonance combined with shakeup.

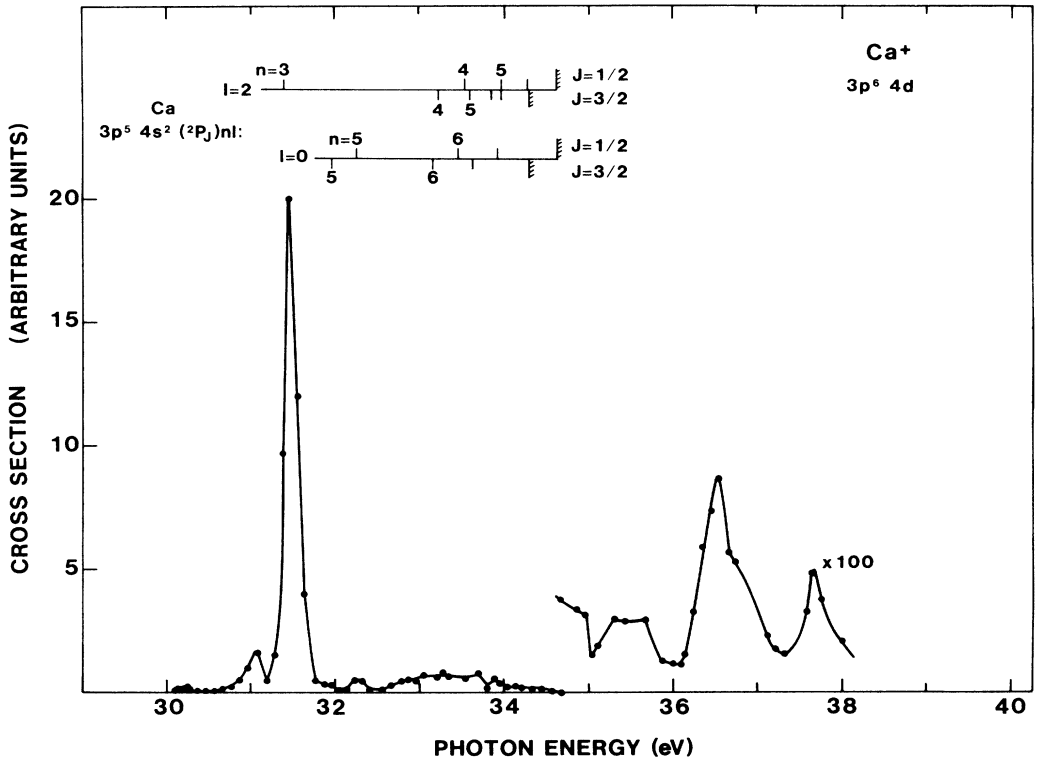

FIG. 19. Variation of the photoionization cross section for production of the $3p^6 4d$ excited state of Ca^{1+} ions.

F. Some comments regarding the higher $3p^6 nl$ cross sections

Figure 1 gives an excellent illustration of the behavior of the entire satellite and Auger spectrum. At 37.66 eV photon energy, we are in the neighborhood of the broad, prominent window resonance (Fig. 10). Moreover, we are just above the threshold for the first of the $3p$ satellites marked D, and at the same time we are in the region of discrete (unresolved) resonances (e.g., $3p^5 4s\,3dnl$) converging to the threshold of the second D satellite. In this region the Auger decay of the $3p$ hole should be quite rapid

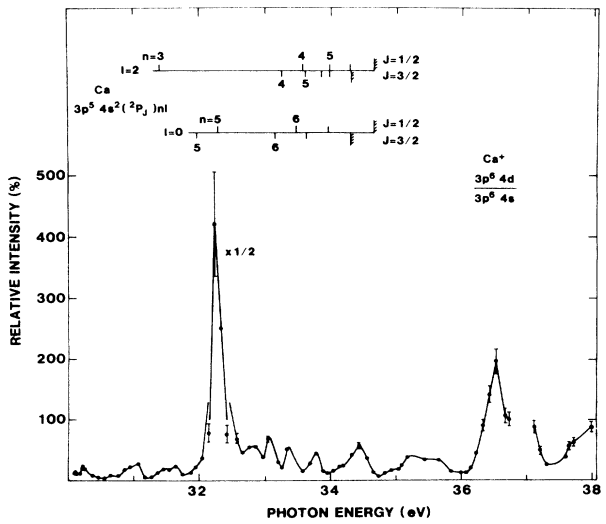

FIG. 20. Variation of the branching ratio between the $3p^6 4d$ PE satellite and the main $3p^6 4s$ line.

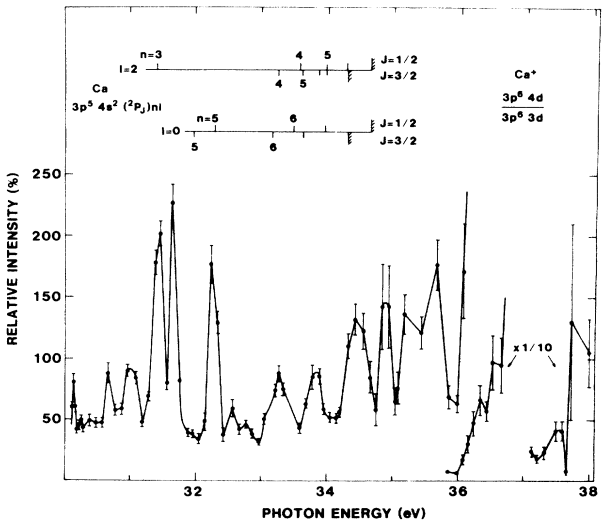

FIG. 21. Variation of the branching ratio between the $3p^6 4d$ and $3p^6 3d$ PE satellites. These results illustrate the different nature of the mechanisms giving rise to both final states of Ca^{1+} ions.

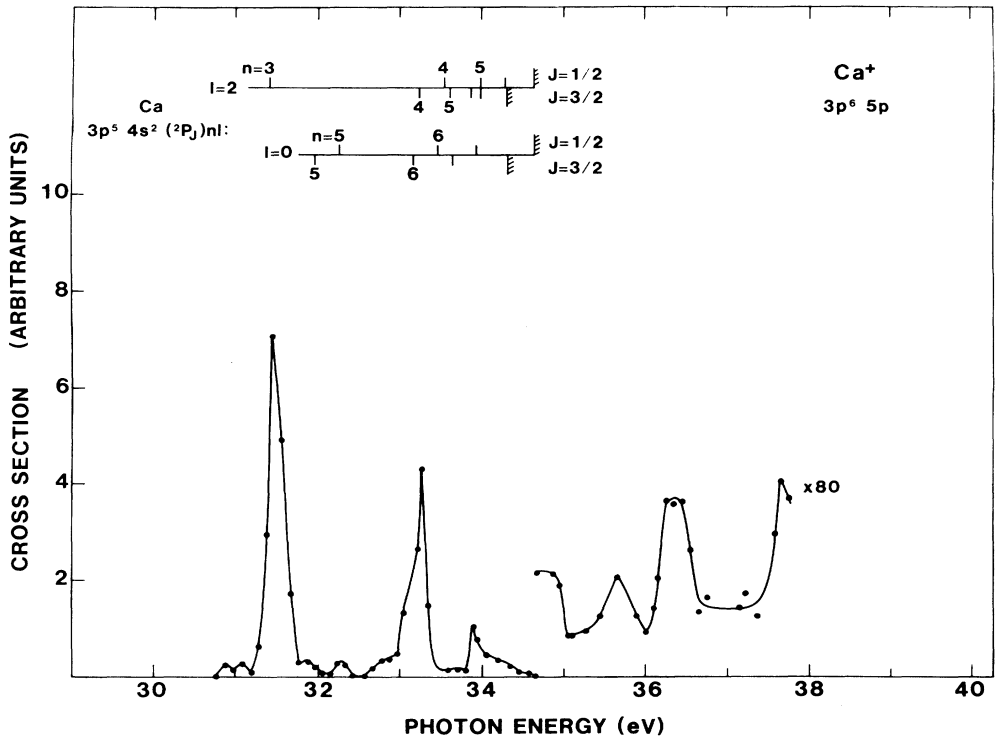

FIG. 22. Variation of the photoionization cross section for production of the $3p^6 5p$ excited state of Ca^{1+} ions.

so that any resonances would mainly branch to the satellite channels. Moreover, there should be resonances converging to the higher satellite thresholds E and F, etc.

There is no particular resonance enhancement of the $4s$ main line or the $3d$ satellite (cf. Figs. 7 and 13) and only weak enhancement of the $4p$ satellite. However, the higher satellites are strongly enhanced *in general.* This could be due to the nonselective manner in which we excite the system; the photon bandpass is approximately 0.3 eV and we are in a region with many resonances converging towards several thresholds. With more selective excitation we would probably find more selectively enhanced Auger lines. Note, however, that there is a natural limit set by the $3p$ Auger width, turning the resonances into a quasicontinuum and the resonant satellites into resonant quasi-Auger lines.[2,64–66]

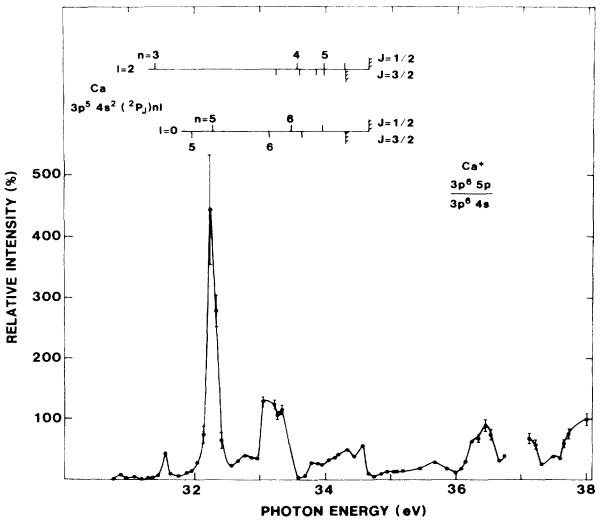

FIG. 23. Variation of the branching ratio between the $3p^6 5p$ PE satellite and the main $3p^6 4s$ line.

In Fig. 1 the structure between 13 and 20 eV on the binding energy scale may now be characterized in the following manner.

(i) Starting at 13 eV, the density of $3p^6 nl$ levels increases towards the left, towards the $Ca^{2+}(3p^6)$ threshold. Between 13 and, say, 16.5 eV the *structure of the spectrum is determined by the* $3p^6 nl$ *structure* and characterized by $4s^{-1}$ PE satellites, whose kinetic energies track the photon energy.

(ii) Between 17 and 18 eV the level density has increased; the $3p$ Auger width now starts to be comparable to the distance between the $3p^6 nl$ levels, making it difficult to resolve the 17-eV structure made up from $6f, 7d, 7f$ levels (and probably some other ones).

(iii) Finally, around 18 eV (still below the $3p^6$ threshold) the $3p$ Auger width dominates; *the* $3p^6 nl$ *structure no longer determines the structure of the spectrum,* and a $3p$ quasi-Auger structure has developed. One can regard this Auger structure as occuring at *fixed kinetic energy* but with a distorted line shape; on the time scale of the Auger decay, one cannot distinguish between highly excited $3p \rightarrow nl$ discrete transitions and $3p \rightarrow \epsilon l$ continuum transitions. One may therefore talk about post-collision interac-

tion (PCI) also below threshold,[2,64–66] and there is a continuous transition of this phenomenon across threshold. The peak at 18 eV binding energy in Fig. 1 is therefore the second of the (PCI shifted) D satellites.

VI. $3p$ SATELLITE CROSS SECTIONS

In order to understand the dynamics of $3p$ ionization, one must know the excitation cross sections also of the $3p^{-1}$ satellites. These satellite cross sections reveal in a sensitive way the presence of resonances and ionization thresholds, and they are also needed for constructing the $3p$-subshell cross section.

Since any excited state of the Ca^{1+} ion is a threshold for an ionization continuum (cf. Fig. 5), one has to deal with a complicated mixture of interacting continua in describing the various partial cross sections. This is easy to understand in principle but very difficult to calculate in practice in any detail. Theoretically, one will therefore have to limit oneself to realistic model calculations involving the most important levels (satellites). This should be enough for understanding the physics; if precise data are needed, they will have to come from experiment.

The $3p^{-1}$ satellite cross section can, in principle, be deduced either directly from the intensity variations of the $3p$ photoelectron satellites (Table II), or indirectly from the $3p$ Auger-electron satellites (Tables III). In practice, we have used the AE spectrum for studying the $3p$ shakedown and shakeup satellites (and main lines) in the 31–40-eV photon-energy range (Figs. 24–26), and the PE spectrum for studying the shakeup satellites in the 40–120-eV photon-energy range (Figs. 27–30).

A. Presentation of experimental results

In the present work, the $3p$ Auger line with the lowest kinetic energy is observed at 13.0 eV, which corresponds to the lowest observed $3p^{-1}$ shakedown satellite, at 31.0 eV binding energy. This coincides with the $3p^5 3d(^3P)4s\ ^4P$ Ca^{1+} level, according to Mansfield and Ottley[8] (see also Table III).

Figure 24 shows the excitation curve (cross section) for the Auger line A_1 at 13.0 eV kinetic energy. As discussed before, this also gives the cross section for, as far as we find, the *lowest-energy* $3p^{-1}$ *shakedown PE satellite,* i.e., the partial ionization cross section for the Ca^{1+} $3p^5 3d(^3P)4s\ ^4P$ level. We note that this ionization cross section has an appearance similar to the various $4s$ (main-line and satellite) partial cross sections.

This is a very special situation, that a $3p^{-1}$ ionization cross section starts below most of the discrete $3p$ single and multiple excitations. Nevertheless, also this $3p^{-1}$ satellite channel must reflect the absorption resonance structure in a manner similar to the $4s^{-1}$ main channel and its satellites. We then note that the similarity to the $3p^6 3d$ cross section is quite striking. The major features are the same, sometimes with slightly different proportions. This similarity appears to be quite reasonable. Most of the suggested excitation and decay mechanisms for these two levels are similar.

In the data of Sato *et al.*[12] the Ca^{2+} curve shows a clear onset at 30.6 eV, with some indication of onset already at 30.2 eV. This onset is probably too strong to be explained by direct (possibly resonant) double ionization. It should therefore give rise to $3p$ Auger lines at 12.2 and 12.6 eV, with lower energy than observed in the present work. The most likely reason for not observing such Auger lines is that their cross sections are far too low for the sensitivity of the present measurement, taking into account the photon flux available. One should compare with the cross section at the onset of the $3p$ AE satellite at 31.0 eV in Fig. 24; the cross section of the unobserved satellite at 30.6 eV should be about 10 times lower.

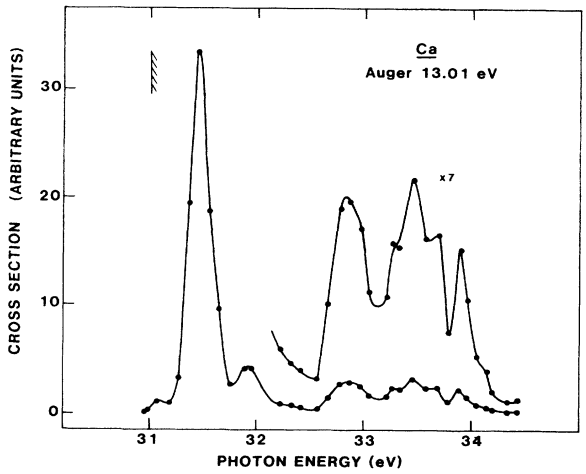

FIG. 24. Variation of the photoionization cross section for production of the first shakedown satellite A_1 observable in this work. The corresponding Ca^{1+*} final state is $3p^5 3d(^3P)4s\ ^4P$, according to Mansfield and Ottley.[8] The ionization threshold, 31.0 eV, is marked in the figure. In this figure, as in Figs. 25 and 26, the data are obtained from the intensity of Auger lines.

Figure 25 shows the *sum of the shakedown and shakeup* $3p^{-1}$ *satellites* (from the Auger spectrum) versus photon energy in the resonance region. Between the A_1 and A_2 thresholds, Figs. 24 and 25 are identical. At each subsequent threshold A_2, A_3, . . . , a new $3p^{-1}$ satellite is added; however, since the absorption strength is not increasing, this means that the $3p^{-1}$ PE emission takes over more and more of the absorption, reducing $4s^{-1}$ channels (cf. Sec. III). Around 34 eV the main $3p^{-1}$ emission channels open up, leading to a large drop of the intensity of the $3p^{-1}$ shakedown satellites, as well as of the $4s$ emission.

Figure 26 presents the ratio of $3p^{-1}$ satellites to main lines; the *total ratio* is given in Fig. 26(a) and the division into shakeup and shakedown contributions in Figs. 26(b) and 26(c). *The satellite strength is clearly very important,* and has to be taken into account when comparing theory and experiment. As mentioned before, the structure in the branching ratios in Fig. 26 cannot be interpreted without knowledge of the absolute variations of the cross sections. For instance, the peak at 37.15 eV appears as a dip in the cross sections. Some of the structure is probably due to

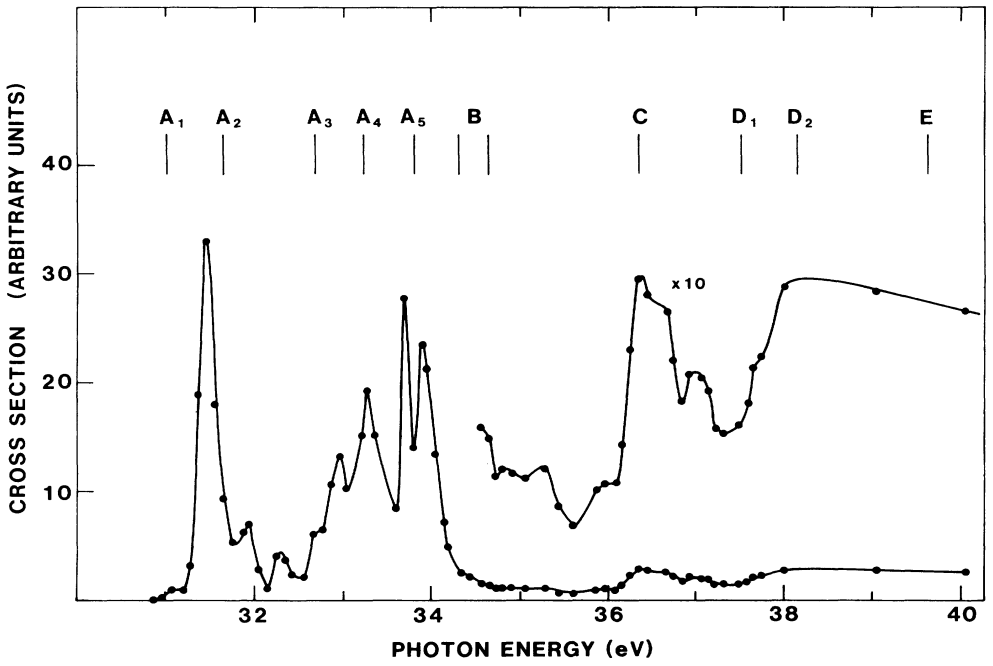

FIG. 25. Variation of the partial photoionization cross section for production of all $3p^{-1}$ shakedown and shakeup satellites in the $3p$ resonance region. The most important $3p$-ionization thresholds are marked in the upper part of the figure.

thresholds rather than to resonances.

The intensity variation of the $3p^{-1}$ shakeup satellites above 40 eV photon energy is shown in Figs. 27–30. The lines through the experimental points only serve to guide the eye; the roughly constant values between 50 and 70 eV in Fig. 30 may therefore be an artifact. Important energy regions could not be studied due to overlap with Auger lines; the 50–70-eV region is missing for all of the satellites, and the 80–130-eV region is missing for the C satellite. Therefore, it is difficult to draw any firm conclusions about the character of the satellites from their energy dependence.

From Fig. 9 it is clear that there is resonance structure in the 70–75-eV region. We have already noted that this could be due to double excitations involving $3p$ and $3s$ electrons. In addition, excitations like $3p^4 4s^2 nln'l'$ can be accompanied by, e.g., $4s \rightarrow 3d$, $4s \rightarrow 5s$, $4s^2 \rightarrow 3d^2$, and $4s^2 \rightarrow 4p^2$ transitions, arising from interactions in the initial and/or final states. It is therefore reasonable to expect resonances of the type

$$3s^2 3p^4(4s^2+4s\,3d+3d^2+4p^2+4s\,5s)nln'l' , \quad (6.1a)$$

$$3s\,3p^5(4s^2+4s\,3d+3d^2+4p^2+4s\,5s)nln'l' , \quad (6.1b)$$

$$3s^0 3p^6(4s^2+4s\,3d+3d^2+4p^2+4s\,5s)nln'l' . \quad (6.1c)$$

These resonances would primarily decay via Coster-Kroning or super-Coster-Kronig decay of one of the $3p$ or $3s$ holes, leading to $3p^{-1}$ and $3s^{-1}$ satellite levels. If the $nln'l'$ orbitals are highly excited, the typical decay scheme would be

$$3p^4(4s^2+3d\,4s+3d^2+4p^2+4s\,5s)nln'l' \rightarrow 3p^5 mlm'l'\epsilon l . \quad (6.2)$$

However, one can expect the most prominent resonances to involve low-lying orbitals like $nl,n'l'=3d,4p$. In the case of Eq. (6.1a) we can then have the following typical decay schemes:

$$3p^4 4s^2 3d\,4p \rightarrow 3p^5 4s\,4p\epsilon l , \quad (6.3a)$$

$$3p^4 4s\,3d^2 4p \rightarrow 3p^5 4s\,4p\epsilon l , \quad (6.3b)$$

$$3p^4 3d^3 4p \rightarrow 3p^5 3d\,4p\epsilon l , \quad (6.3c)$$

$$3p^4 3d^3 4p \rightarrow 3p^5 3d^2\epsilon l , \quad (6.3d)$$

$$3p^4 3d\,4p^3 \rightarrow 3p^5 4p^2\epsilon l , \quad (6.3e)$$

$$3p^4 4s\,5s\,3d\,4p \rightarrow 3p^5 4s\,5s\epsilon l , \quad (6.3f)$$

$$3p^4 4s\,5s\,3d\,4p \rightarrow 3p^5 4p\,5s\epsilon l . \quad (6.3g)$$

Equation (6.3) describes highly selective, resonant enhancement of a great number of $3p^{-1}$ satellites (note that there are further possibilities if we include less prominent decay channels). Several of the experimentally observed $3p^{-1}$ satellites are quite prominent (see, e.g., Fig. 2). Although some of these satellites have not been properly identified, they should primarily belong to the configurations appearing in Eq. (6.3).

Figure 27 shows the intensity variation of the first shakeup satellite C at 36 eV binding energy. According to Mansfield and Newsom,[7] this satellite may possibly be

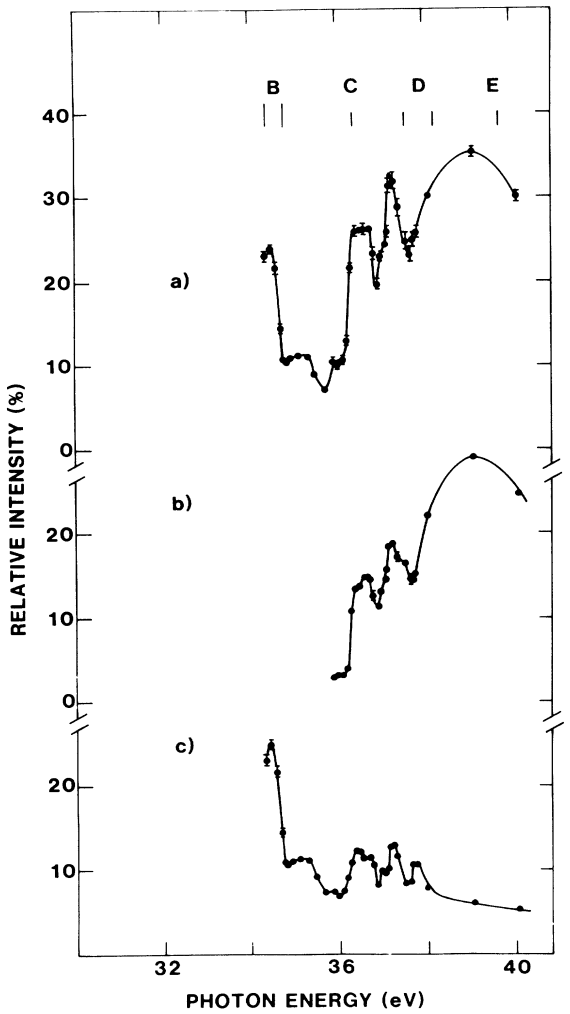

FIG. 26. Variation of the branching ratio between the $3p^{-1}$ PE satellite and the main $3p^5 4s^2\,^2P_{1/2,3/2}$ lines: (a) is the ratio for all satellites, (b) is the ratio for the shakeup, and (c) is the ratio for the shakedown contributions.

classified as $3p^5 3d^2$. The absolute cross-section determination is related to the main $3p$ lines. In the region which could be studied, the overall intensity variation is very similar to that of the $3p$ main lines. This is demonstrated by the roughly constant average level of the branching ratio in Fig. 28. The prominent structure is mainly due to intensity variation of the satellite itself, and is probably associated with multiple-electron excitations.

The intensity of satellite C starts with a high value at threshold. This is evident from a PE-AE spectrum at 36.54 eV photon energy,[2,21] and from the $3p$ satellite-to-main-line ratio shown in Fig. 26(b). The satellite C is thus born as discrete multiple-excitation resonances below its own threshold (excitation with shakeup), and crosses into the true continuum with full strength (ionization with shakeup).

A similar type of behavior is shown by the E satellite in

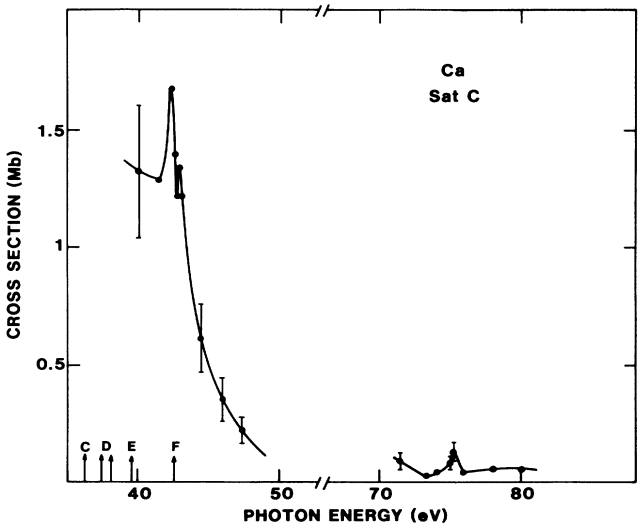

FIG. 27. Variation of the partial photoionization cross section for production of the shakeup satellite C at 36.3 eV binding energy [final state of the Ca^{1+*} ion is $3p^5(3d^2\,^1S_0)^2P_{1/2,3/2}$ according to Mansfield and Ottley (Ref. 8); see Table II].

Figs. 29 and 30 (we tentatively classify it as $3p^5 4s4p$; however, $3p^5 4p^2$ would also be a possibility). The intensity of the E satellite follows the rapid drop of the $3p$ main line down towards the minimum around 60 eV in the $3p$ cross section, as demonstrated by the roughly constant (on the average slowly decreasing) ratio in Fig. 30. In particular, the ratio is quite high close to the threshold of the E satellite. The markedly low intensity in the 70–120-eV range could be due to resonance and interference effects

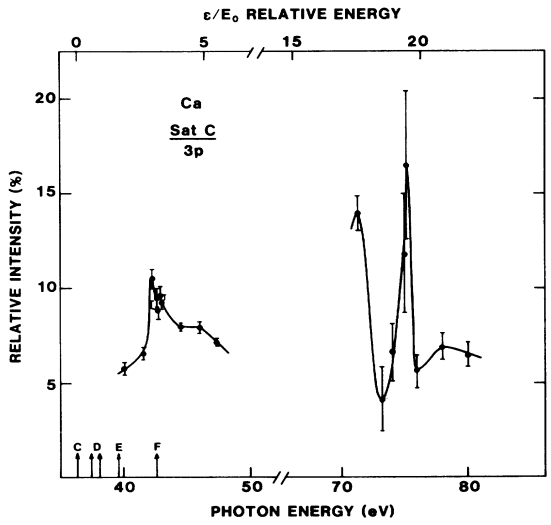

FIG. 28. Variation in the branching ratio between the shakeup satellite C and the main $3p^5 4s^2\,^2P_{1/2,3/2}$ lines. The upper scale of the figure shows the ratio between the excess energy available (kinetic energy of the shakeup electrons) and the shakeup energy (energy difference between the satellite and the main $3p^5 4s^2\,^2P_{3/2}$ line).

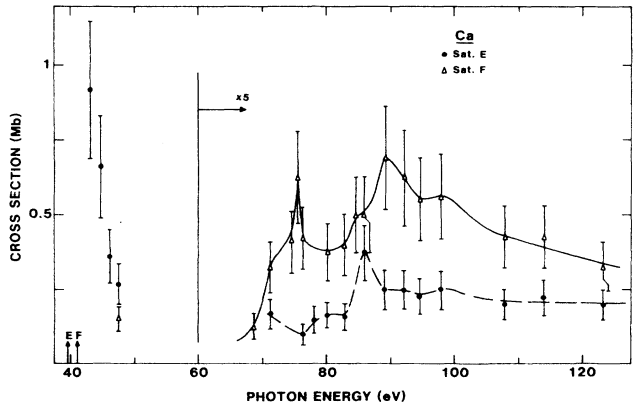

FIG. 29. Variation of the partial photoionization cross section for producing the shakeup satellites E [●; binding energy is 39.6 eV; the final state is (tentatively) $3p^5 4s\,4p$] and F [△; binding energy is 42.6 eV; the final state is (probably) $3p^5 4s\,5s$].

(losses to other channels; cf. Sec. IV B and Fig. 9). It should be emphasized, however, that the absence of data points in the 50—70-eV range is quite embarassing and prevents us both from characterizing the threshold behavior of the E satellite and from understanding how the threshold behavior develops into the high-energy behavior above 70 eV.

The F satellite ($3p^5 4s\,5s$) is only represented by a single point near its threshold. The overall variation of the branching ratio in Fig. 30, however, suggests that the ratio has a nonzero (actually fairly high) value near threshold and then slowly *grows towards higher energies.* This is precisely what one would expect for a monopole shakeup

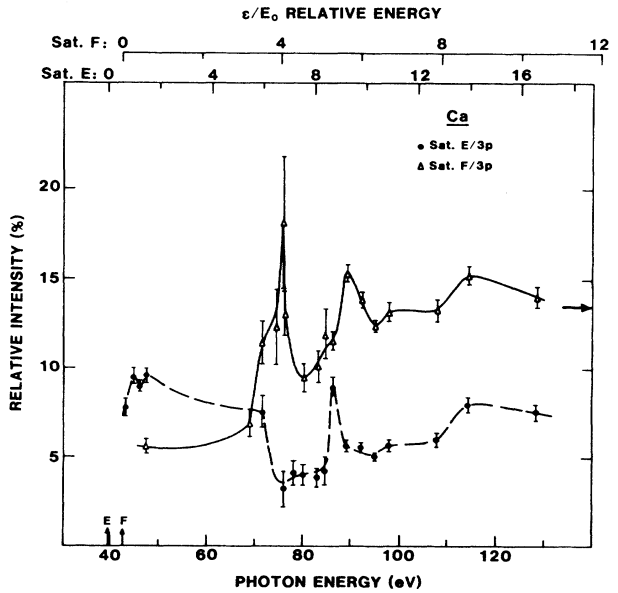

FIG. 30. Variation in the branching ratio between the shakeup satellites E (●) and F (△) and the main $3p^5 4s^2\,{}^2P_{1/2,3/2}$ lines.

satellite in an atomic system: Close to threshold the photoelectron will partly screen the core hole and thus reduce the shakeup intensity relative to high energies. However, the intensity will not go to zero approaching the threshold because of the discrete structure below threshold ($3p \rightarrow nl$ excitation with $4s \rightarrow 5s$ shakeup).

The intensity of the E satellite, on the other hand, is quite large near threshold and slowly *decreases,* on the average, towards higher energies. This is consistent with the (proposed) character of the E satellite of *nonshakeup* ($3p^5 4s\,4p$), excited by inelastic scattering, and via different correlation processes. However, we note again the uncertainty in our conclusions: If we only regard the 75—130-eV region of the $R(E/3p)$ ratio in Fig. 30, the average behavior is quite similar to the $R(F/3p)$ ratio, suggesting a shakeup origin of the E satellite.

In Fig. 30 we have also marked the theoretical satellite-to-main-line ratio $R(F/3p)=13.5\%$ calculated by Walter and Schirmer[19] in the sudden limit (infinite kinetic energy). The agreement is very good in spite of the many complications in this energy range. At around 120 eV photon energy the kinetic energy is about ten times the $4s$-$5s$ shakeup energy. We should therefore be in the sudden limit with respect to this excitation, and would expect the F-satellite intensity to grow from a finite value at threshold towards the sudden limit from below. However, as discussed in Sec. IV B, there are many resonances and thresholds in the 70—120-eV region associated with two-electron excitations from the $3p$ and $3s$ shells, which will influence the absolute intensities of both satellites and the main $3p$ lines.

In Fig. 9 we have already established that in the 90—120-eV range the main $3p$ lines must have lost considerable intensity to unobserved high-energy satellites ($3p^{-2}nl$, $3p^{-1}3s^{-1}nl$, $3s^{-2}nl$). We suggest that this lowering of the $3p$ main-line intensity is the main reason the $R(F/3p)$ ratio being larger than expected theoretically for a shakeup process. The overall impression is therefore that the F satellite indeed behaves like a shakeup satellite.

This question of normalization must also influence the E satellite in the same way, making it roughly constant from 90 up to 130 eV. This behavior is evident from the absolute variation in Fig. 29.

In Fig. 30 the average variation of the ratio of the E satellite to the main $3p$ line (or better, the $3p$ total intensity) is not that of a shakeup line. This then does not contradict our suggestion of a satellite configuration $E(3p^5 4s\,4p)$, which cannot be excited by a suddenly created $3p$ core hole. In fact, the suggested configuration allows us to consider the level as a Coster-Kronig satellite to the $3s$ hole. The possibilities of excitation are inelastic scattering, virtual excitation and Coster-Kronig decay of a $3s$ hole, and $3p$-$4s$ correlation. The resonance structure in the 70—90-eV region has not been identified. However, as discussed in Sec. IV, it is easy to imagine that double excitations like $3p^{-2}3d4p$ should play an important role.

Finally, we have not been able to detect what we would expect to be a windowlike $3s \rightarrow 4p$ transition between 45 and 50 eV photon energy.[2] The oscillator strength of the transition is probably too weak to allow detection with the present photon flux and counting times.

B. Connection with Ca^{1+} and Ca^{2+} ion yield cross sections

The excitation cross section for the accumulated sum of $3p^{-1}$ Auger *satellites* in Fig. 25 also represents the cross section for the yield of Ca^{2+} ions from 31 to 34.3 eV (threshold for $3p^5 4s^2$). This is because the final state of the Auger process is Ca^{2+} ions, and because direct double ionization is negligible. In the same way, Fig. 10 shows the excitation cross section for the accumulated sum of $3p^{-1}$ Auger *main lines and satellites,* which also represents the cross section for the yield of Ca^{2+} ions from 34.3 to 40 eV.

Combining Fig. 25 and Fig. 10 then effectively gives the Ca^{2+} excitation cross section in the 31–40-eV photon-energy region. In the 31–36-eV range, the resulting curve is *very similar* to the Ca^{2+} yield directly measured by Sato *et al.*[12] (whose measurements do not extend above 36 eV). The good agreement shows that there is a high degree of consistency between the present results and those of Sato *et al.*,[12] and it indicates that the different partial cross sections of this work are quite reliable. The differences (an apparent lack of details in the present data) can be ascribed to the simple fact that we have sampled the spectrum using relatively few points in photon energy in the resonance region. The experimental resolution in the two experiments is essentially the same.

C. Further comparison with theoretical calculations

So far, we have compared theoretical continuum cross sections[2,13–15] above the $3p$ threshold with the experimental results, as shown in Figs. 9 and 10. With the present normalization to the LDRPA calculation, integration of the experimental cross section from the $3p$ threshold and upwards gives an *effective number of electrons equal to 3.2.* Of course, this result essentially reflects the theoretical value, since the fit between theory and experiment is very good on the average.

The normalization of the $3p$ cross section establishes an absolute cross-section scale. On this scale, the area of the $3p^5 4s^2 3d\ ^1P$ giant dipole resonance at 31.41 eV contributes approximately 1 *effective electron* to the oscillator-strength sum. However, this value is quite uncertain, perhaps by as much as a factor of 2. The RPAE predicts,[13] in fact, a value of more than 2. A similar theoretical result is true for the $5p \rightarrow 5d$ transition in barium.[13,22]

Among the theoretical calculations, only Altun, Carter, and Kelly[15] present a ($4s$) continuum cross section in the $3p^5 4s^2 3d\ ^1P$ and $3p^5 4s^2 nd,ns$ resonance region.[56] This corresponds formally to the $4s$-subshell cross section (main lines plus satellites), which represents the theoretical absorption cross section. However, in the present situation there are $3p^{-1}$ shakedown satellite continua underneath the $3p \rightarrow 3d$ resonance which are not taken into account by the calculation. In this case, only theoretical and experimental cross sections equivalent to absorption (total) cross sections can be directly compared, because the theoretical and experimental partial (even subshell) cross sections do not describe the same thing.

More explicitly, the results of Altun, Carter, and Kelly[15] must be compared with the photon-energy variation of the total ion yield (Ca^{1+} plus Ca^{2+}). The Ca^{1+} yield ($4s$-subshell cross section) is not enough because in the experiment, but not in the calculation, intensity is lost to the Ca^{2+} channel. For a comparison with the present experimental data we must add the cross sections of the $4s^{-1}$ main line (Figs. 6 and 7), the $4s^{-1}$ satellites (Fig. 6, plus others, not shown), and the $3p^{-1}$ satellites (Fig. 24).

Comparing the results of Altun, Carter, and Kelly[15] with the Ca-ion yield[12] we note that the calculated $3p \rightarrow 3d$ line profile has the correct general appearance, i.e., an asymmetric Fano profile with a interference minimum (zero) around 32.5 eV. Looking in greater detail, we have the impression that this type of calculation predicts a more pronounced asymmetry than observed. This might be due to the presence of all the $4s$-satellite continua, and to the triple excitations sharing intensity with the $3p \rightarrow 3d$ resonance. In fact, it seems to us from the present experiments (see, e.g., Fig. 6) that the $4s$ and $3p$ satellite cross sections are more symmetric than the cross section of the $4s$ main line.

In retrospect, when it comes to *line shapes,* the most relevant thing is probably after all to compare the calculated $3p \rightarrow 3d$ line profile (from Ref. 15, or from RPA types of calculations) with the profile in the experimental $4s$ *main-line* cross section; it is the character of the wave functions which determines the effects of interference. However, when it comes to *intensities,* the strength of the resonance of the $4s$ main line will be less than the strength of the corresponding resonance in the absorption (total) cross section.

Finally, we would like to comment on some recent theoretical calculations[17,18] of the variation of the intensity of the Ca^{1+*} $3p^6 3d$ and $3p^6 4p$ levels ($4s^{-1}$ satellites) with photon energy. Both investigations deal with the behavior from low photon energies up to 30 eV. In addition, Altun and Kelly[17] calculate the resonance behavior of the satellites in the region of the $3p^5 4s^2 3d\ ^1P$ giant dipole resonance.

Comparing the calculated $3d$ and $4p$ satellite line profiles[17] and the $R(3d/4s)$ and $R(4p/4s)$ branching ratios[17,18] with the experimental results in Secs. V A and V B, we have to conclude that the agreement is not good. It is not surprising that the line profiles do not agree with experiment; apart from any theoretical problems, the mixture of the $3p^5 4s^2 3d\ ^1P$ giant dipole resonance with triple excitations makes it difficult to identify experimentally any line profile at all.

A greater problem is, in our opinion, that the calculated $R(3d/4s)$ and $R(4p/4s)$ branching ratios do not agree with the present experimental results. This does not seem to be a problem confined to the $3p^5 4s^2 3d\ ^1P$ resonance region. Experimentally we find that the $R(3d/4s)$ and $R(4p/4s)$ branching ratios (Figs. 14 and 16) are *roughly equal* and *roughly constant* in the 28–32-eV region (if one disregards multiply excited resonances, which decay in selective ways). In contrast, off resonance, both calculations[17,18] predict the $R(4p/4s)$ ratio to be about five times larger (or more) than the $R(3d/4s)$ ratio, and in the $3p^5 4s^2 3d\ ^1P$ resonance region the ratios seem to vary appreciably.[17]

Very recently, Hansen and Scott[67] have improved the

calculation by Cowan, Hansen, and Smid[18] by including final-state interaction within an R-matrix calculation, in particular interaction between the $4s^{-1}\epsilon p$ and $4s^{-2}4p\epsilon l$ continuum channels. As a result, there is now reasonable agreement with Altun and Kelly[17] regarding the shapes and magnitudes of the cross sections of the $4s$ main line and $3d$ and $4p$ satellites. It seems that Hansen and Scott[67] agree somewhat better with experiment[6] at 21.2 eV, in particular regarding the $R(4p/3d)$ ratio which seems to be around two in the 21–26-eV range.[67] However, there is no indication how the branching ratios will develop closer to resonance.

We believe that some important aspects are still missing from the theoretical treatments so far, in particular in what concerns the effects of the $3p^{-1}3d\ ^1P$ resonance (in fact, the entire $3p^{-1}nd,\epsilon d\ ^1P$ channel). Not having performed any numerical calculations yet, we can only offer some suggestions.

In spite of the poor-to-fair agreement between calculations and experiment, we also believe that the $3d$ and $4p$ satellites are created via $4s^2 \rightarrow d^2$ ($md\,3d$) and $4s^2 \rightarrow p^2$ ($mp\,4p$) ground- (initial-) state correlation with important contributions from final-state continuum interaction (e.g., inelastic scattering, conjugate shakeup). If we only consider explicitly the ground-state-correlation part, the essential lowest-order contributions to the ionization amplitudes will be [Fig. 31(b)]

$$t_\epsilon^{3d}(\omega)=\sum_m \frac{\langle \epsilon \mid r(\omega) \mid md \rangle \langle md\,3d \mid 1/r_{12} \mid 4s\,4s \rangle}{\epsilon_{md}+\epsilon_{3d}-\epsilon_{4s}-\epsilon_{4s}}\ , \tag{6.4}$$

$$t_\epsilon^{4p}(\omega)=\sum_m \frac{\langle \epsilon \mid r(\omega) \mid mp \rangle \langle mp\,4p \mid 1/r_{12} \mid 4s\,4s \rangle}{\epsilon_{mp}+\epsilon_{4p}-\epsilon_{4s}-\epsilon_{4s}}\ . \tag{6.5}$$

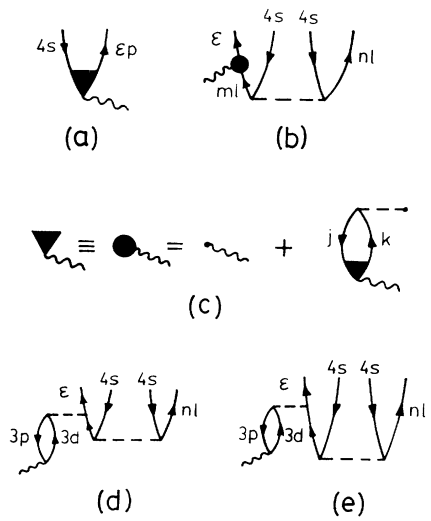

FIG. 31. Diagrammatic representations of photoionization amplitudes within an RPA description of the screened electron-photon dipole interaction: (a) $4s$ ionization, $3p^6 4s$ final state; (b) $4s$ ionization with excitation, $3p^6 nl$ final state ($nl=3d,4p,\ldots$); (c) effective (screened) dipole interaction within the RPA; (d) and (e) lowest-order contributions to the effective process in (b).

In Eqs. (6.4) and (6.5) the photoionization matrix element is *screened* and is given by the RPA (LDRPA, RPAE, RRPA) [Fig. 31(c)]. These expressions exactly represent the sum of the diagrams in Figs. 31(d) and 31(e) (cf. two-photon ionization;[68] also note that in a more complete treatment, inclusion of the Coulomb interaction introduces triply-excited intermediate resonances). The important thing is that the screened interaction $r(\omega)$ (Refs. 2 and 3) incorporates the $3p \rightarrow 3d$ resonance in a systematic manner, including the interference between the direct and resonant terms.

Comparing with Altun and Kelly[17] we note that they have included the screened (correlated, in their terms) dipole matrix element in many different diagrams. However, as far as we can see, they have not included it in the diagrams giving the ground-state-correlation amplitudes in Eqs. (6.4) and (6.5). We suspect that this resonance contribution to the $3d$ and $4p$ satellites is very important, and would most certainly change the resonance-line profiles.

Equations (6.4) and (6.5) most certainly represent essential contributions to the satellite-ionization amplitudes. Moreover, one should add the appropriate processes representing final-state interaction,[17] in particular, the $4s^{-1}\epsilon p - 4s^{-2}4p\epsilon l$ scattering process,[17,67] driven by the same screened (effective) dipole operator $r(\omega)$ as the ground-state correlation processes. Whether introduction of the effective dipole operator will improve the *relative* intensities of the $3d$ and $4p$ satellites remains to be investigated. However, we note that since the ionization amplitude for the main $4s$ line [Fig. 31(c)] is given by

$$t_\epsilon^{4s}(\omega)=\langle \epsilon \mid r(\omega) \mid 4s \rangle\ , \tag{6.6}$$

the *resonance cancels in the branching ratios,*

$$R(3d/4s)=\mid t_\epsilon^{3d}(\omega)/t_\epsilon^{4s}(\omega) \mid^2\ , \tag{6.7}$$

$$R(4p/4s)=\mid t_\epsilon^{4p}(\omega)/t_\epsilon^{4s}(\omega) \mid^2\ . \tag{6.8}$$

Even well outside the very resonance, the "resonant" part, which involves the $3p$-$3d$ core excitation, tends to dominate the effective (correlated) dipole matrix elements (e.g., the $4s$ partial cross section). Therefore, it seems plausible that the cancellation should extend to a range of photon energies well off resonance. Consequently, the branching ratios should vary very slowly (essentially not at all) between the on- and off-resonance situations.

Finally, if it is true that Altun and Kelly[17] have not used the $3p$-$3d$-correlated (RPAE screened) matrix element for calculating the amplitude in Fig. 31(b) and Eqs. (6.4) and (6.5), then there is a good chance that the present scheme will, in fact, represent one of the basic elements of a correct description of the satellite-photoionization cross sections both off resonance and at the $3p^5 4s^2 3d\ ^1P$ resonance. Note, however, that deviations from this simple behavior can be clearly seen in the satellite-to-satellite branching ratios, e.g., $R(4d/3d)$ in Fig. 21, where the $3p^5 4s^2 3d\ ^1P$ resonance shows up loud and clear. Also note that all other resonances, in particular, multiply-excited ones, show a more selective behavior, with clear differences in the transition amplitudes due to different excitations mechanisms on and off resonance. This is

why there are resonances in the branching ratios, although the resonance function has cancelled out.

VII. SUMMARY AND CONCLUDING REMARKS

Photoionization of the $4s$, $3p$, and $3s$ subshells of atomic calcium has been studied experimentally by applying the electron spectroscopy using synchrotron radiation (ESSR) technique in the 26—120-eV photon-energy region. The experimental results have been analyzed with the help of theoretical calculations (local-density random-phase approximation, LDRPA; relativistic random-phase approximation RRPA). The interpretation of the experimental results has also been supported by other types of model calculations within the framework of many-electron theory.

Experimentally, we have paid particular attention to the region around the $3p$ thresholds where resonant excitations of a $3p$-subshell electron occur. Auger electrons following the decay of a $3p$ or $3s$ hole have been observed; this includes decay of excited states of the $Ca^{1+}(3p^{-1})$ ion, which have been identified. Moreover, for the first time the binding energy of the $3s$ electron has been measured in atomic calcium.

Placing our intensity measurements on an absolute scale by normalizing them to our calculated LDRPA $3p$-subshell photoionization cross section, we have found the resulting measured absolute partial cross sections to be in good agreement with the many-body calculations. Both the LDRPA and the RRPA (RPAE) describe the average experimental partial cross sections quite well. Nevertheless, the sometimes dramatic differences between experiment and calculations clearly demonstrate that the theoretical approach must be extended to include the dynamics of multiple excitations in both excitation and ionization.

We have also confirmed that electron spectroscopy is a powerful tool for studying resonant excitation and decay processes in the $3p$-threshold region. In general, any given intermediate $3p$ resonance will lead to resonant enhancement of large groups of photoelectron lines, the distribution of which characterizes the intermediate state. However, in some exceptional cases does a resonance appear only in one or two specific satellite lines, giving direct clues to the identity of the intermediate state.

An improvement of the present experimental study would require the use of angle-resolved electron spectroscopy in connection with an increased resolution of the monochromatic photon beam. This would offer a better characterization of the excited states of the Ca^{1+} ion, and would allow further tests of theoretical calculations. In the same way, the use of coincidence techniques would help to suppress the overlap of AE and PE lines in the photoelectron spectra.

An improvement of existing theoretical treatments requires systematic inclusion of the dynamics of multiple excitations in both excitation and ionization in, as it seems, the entire 25—120-eV photon-energy region.

Finally, this work emphasizes the need for more determinations of absolute total photoabsorption cross sections for metal vapors. This would allow a more rigorous comparison of experiments and theory on an absolute scale.

ACKNOWLEDGMENTS

We would like to thank P. Dhez for assisting with the measurements and S. Salomonson for a critical reading of the manuscript. Thanks are also due to the technical staff of the Laboratoire pour l'Utilisation du Rayonnement Electromagnétique (LURE) for their service and cooperation. This work was supported by the Centre National de la Recherche Scientifique, the Université de Paris—Sud (Orsay, France), and the Swedish Natural Science Research Council.

[1]J. M. Bizau, P. Gérard, F. J. Wuilleumier, and G. Wendin, Phys. Rev. Lett. **53**, 2083 (1984).

[2](a) G. Wendin, in *New Trends in Atomic Physics*, 1982 Les Houches Lectures, Session XXXVIII, edited by G. Grynberg and R. Stora (Elsevier, New York, 1984), and references therein; (b) Comments At. Mol. Phys. **17**, 115 (1986), and references therein.

[3]G. Wendin, Phys. Rev. Lett. **53**, 724 (1984).

[4]G. Wendin, Struct. Bonding (Berlin) **45**, 1 (1981), and references therein.

[5]G. Wendin, in *Photoionization of Atoms and Molecules*, edited by B. Buckley, Daresbury Laboratory Report No. DL/SCI/R11, 1978 (unpublished).

[6](a) S. Süzer, S. T. Lee, and D. A. Shirley, Phys. Rev. A **13**, 1842 (1976); (b) E. P. F. Lee, and A. W. Potts, J. Phys. B **14**, L61 (1981).

[7]M. W. D. Mansfield, and G. H. Newsom, Proc. R. Soc. London, Sec. A **357**, 77 (1977).

[8]M. W. D. Mansfield, and T. W. Ottley, Proc. R. Soc. London, Sec. A **365**, 413 (1979).

[9]J. P. Connerade, M. A. Baig, W. R. S. Garton, and G. H. Newsom, Proc. R. Soc. London, Sec. A **371**, 295 (1980).

[10](a) W. Schmitz, B. Breuckmann, and W. Mehlhorn, J. Phys. B **9**, L493 (1976); (b) V. Pejcev, T. W. Ottley, D. Rassi, and K. J. Ross, *ibid.* **11**, 531 (1978).

[11]D. M. P. Holland and K. Codling, J. Phys. B **14**, 2345 (1981).

[12]Y. Sato, T. Hyaishi, Y. Itikawa, Y. Itoh, J. Murakami, T. Nagata, T. Sasaki, B. Sonntag, A. Yagishita, and M. Yoshimo, J. Phys. B **18**, 225 (1985).

[13]M. Ya. Amusia, and N. A. Cherepkov, Case Stud. At. Phys. **5**, 47 (1975).

[14]P. C. Deshmukh, and W. R. Johnson, Phys. Rev. A **27**, 326 (1983).

[15]Z. Altun, S. L. Carter, and H. P. Kelly, Phys. Rev. A **27**, 1943 (1983).

[16]Z. Altun, S. L. Carter, and H. P. Kelly, J. Phys. B **15**, L709 (1982).

[17]Z. Altun, and H. P. Kelly, Phys. Rev. A **31**, 3711 (1985).

[18]R. D. Cowan, J. E. Hansen, and H. Smid, Phys. Rev. A **31**, 2750 (1985).

[19]O. Walter, and J. Schirmer, J. Phys. B **14**, 3805 (1981).

[20](a) J. M. Bizau, F. J. Wuilleumier, P. Dhez, and G. Wendin,

Abstracts of the 8th International Conference on Atomic Physics 1982, Göteborg (unpublished), p. 3; (b) *Abstracts of the International Conference on X-ray and Atomic Inner-Shell Physics, Eugene, Oregon, 1982* (unpublished), p. 151.

[21]F. J. Wuillumier, J. Phys. (Paris) Colloq. **43**, C2-343 (1982).

[22]G. Wendin, in *Vacuum Ultraviolet Radiation,* edited by E. E. Koch, R. Haensel, and C. Kunz (Vieweg/Pergamon, New York, 1974), p. 225.

[23](a) J. P. Connerade, and D. H. Tracy, J. Phys. **10**, L235 (1977); (b) J. P. Connerade, M. W. D. Mansfield, G. H. Newsom, D. H. Tracy, M. A. Baig, and K. Thimm, Philos. Trans. R. Soc. London A **290**, 327 (1979); S. J. Rose, I. Grant, and J. P. Connerade, *ibid.* **296**, 527 (1980).

[24]J. M. Bizau, F. J. Wuilleumier, G. Wendin, and P. Dhez, *Abstracts of the International Conference on X-ray and Atomic Inner-Shell Physics Eugene, Oregon, 1982* (unpublished), p. 153; and (unpublished).

[25]P. H. Kobrin, R. A. Rosenberg, U. Becker, S. Southworth, C. M. Truesdale, D. W. Lindle, G. Thornton, M. G. White, E. D. Polyakoff, and D. A. Shirley, J. Phys. B **16**, 4339 (1983).

[26]D. Cubaynes *et al.* (unpublished).

[27]D. M. P. Holland, K. Codling, and R. N. Chamberlain, J. Phys. B **14**, 839 (1981).

[28]B. Lewandowski, J. Ganz, H. Hotop, and M. W. Ruf, J. Phys. B **14**, L803 (1981).

[29]J. M. Bizau, D. Cubaynes, P. Gérard, F. J. Wuilleumier, J. L. Picqué, D. L. Ederer, B. Carré, and G. Wendin, Phys. Rev. Lett. **57**, 306 (1986).

[30]J. B. West, P. R. Woodruff, K. Codling, and R. G. Houlgate, J. Phys. B **9**, 407 (1976).

[31]F. J. Wuilleumier, M. Y. Adam, P. Dhez, N. Sandner, V. Schmidt, and W. Mehlhorn, Phys. Rev. A **16**, 646 (1977).

[32]R. A. Rosenberg, M. G. White, G. Thornton, and D. A. Shirley, Phys. Rev. Lett. **43**, 327 (1979).

[33]N. Sandner, V. Schmidt, W. Mehlhorn, F. J. Wuilleumier, M. Y. Adam, and J. P. Desclaux, J. Phys. B **13**, 2937 (1980).

[34]E. Schmidt, H. Schröder, B. Sonntag, H. Voss, and M. E. Wetzel, J. Phys. B **18**, 79 (1985).

[35]P. H. Kobrin, S. Southworth, C. M. Truesdale, D. W. Lindle, U. Becker, and D. A. Shirley, Phys. Rev. A **29**, 194 (1984).

[36]M. O. Krause, T. A. Carlsson, and A. Fahlman, Phys. Rev. A **30**, 1316 (1984).

[37]M. O. Krause, F. Cerrina, and A. Fahlman, Phys. Rev. Lett. **50**, 1118 (1983).

[38]M. O. Krause, W. A. Svensson, T. A. Carlson, G. Leroi, D. E. Ederer, D. M. P. Holland, and A. C. Parr, J. Phys. B **18**, 4096 (1985).

[39]U. Becker, H. G. Kerkhoff, D. W. Lindle, P. H. Kobrin, T. A. Ferret, P. A. Heimann, C. M. Truesdale, and D. A. Shirley, Phys. Rev. A **34**, 2858 (1986).

[40]W. A. Svensson, M. O. Krause, T. A. Carlson, V. Radojević, and W. R. Johnson, Phys. Rev. A **33**, 1024 (1986).

[41]M. O. Krause, F. Cerrina, A. Fahlman, and T. A. Carlson, Phys. Rev. Lett. **51**, 2033 (1983).

[42]M. O. Krause, P. Gérard, A. Fahlman, T. A. Carlson, and A. Svensson, Phys. Rev. A **33**, 3146 (1986).

[43]J. Barth, I. Chorkendorff, F. Gerken, C. Kunz, R. Nyholm, J. Schmidt-May, and G. Wendin, Phys. Rev. B **30**, 6251 (1984).

[44]J. P. Ziezel, *Abstracts of the 2nd European Conference on Atomic and Molecular Physics,* 1985, Amsterdam (unpublished), p. 410.

[45]S. Krummacher, V. Schmidt, J. M. Bizau, D. Ederer, P. Dhez, and F. Wuilleumier, J. Phys. B **15**, 4363 (1982).

[46]P. K. Larsen, W. A. M. van Beers, J. M. Bizau, F. J. Wuilleumier, S. Krummacher, V. Schmidt, and D. Ederer, Nucl. Instr. Meth. **195**, 245 (1982).

[47]V. Schmidt, Phys. Lett. **45A**, 63 (1973).

[48]J. Sugar, and C. Corliss, J. Phys. Chem. Ref. Data **8**, 865 (1979).

[49]S. Krummacher, Thesis, Universität Freiburg im Breisgau, 1981 (unpublished).

[50]M. Y. Adam, F. Wuilleumier, N. Sandner, V. Schmidt, S. Krummacher, and W. Mehlhorn, Jpn. J. Appl. Phys. Suppl. **17-2**, 170 (1978).

[51]M. O. Krause, Chem. Phys. Lett. **10**, 65 (1971).

[52]P. R. Woodruff, L. Torop, and J. B. West, J. Electron Spectrosc. Relat. Phenom. **12**, 133 (1977).

[53]The theoretical values of the $3p$ continuum cross section just above the $3p$ threshold is 35—40 Mb and, by continuity, gives the average value of the *3p-absorption* cross section in the discrete region just below threshold. Below the $3p$ threshold this absorption cross section is divided up among the $4s^{-1}$ channels (and the $3p$ shakedown satellite channels). *Just above* threshold the $4s^{-1}$ cross section is about 1 Mb, to which value the $4s^{-1}$ cross section has to drop from the high value below threshold.

[54]Sufficiently close to an asymmetric but narrow resonance one may, of course, always neglect the direct term. However, one then only considers a central, Lorentzian, part of the line profile.

[55]The analogous problem in atomic Ba has been discussed in similar terms by Wendin in Ref. 5 in terms of resonant enhancement of $5p$ shakedown photoelectron satellites, with almost zero kinetic energy, and their mirror-image counterparts in the form of Auger electrons. Also in this case, two-step decay mechanisms involving spin-flip processes only represent one out of several decay paths, and has never been shown to be more important than the recombination mechanism.

[56]Cf. the analogous result for the $5p$-$5d$ transition in Ba [Refs. 2(a) and 22].

[57]M. Y. Adam, P. Morin, and G. Wendin, Phys. Rev. A **31**, 1426 (1985) and references therein.

[58]M. Ya. Amusia, Appl. Opt. **19**, 4042 (1980); *Atomic Physics* edited by I. Lindgren, S. Svanberg, and A. Rosén (Plenum, New York, 1983), Vol. 8, p. 287.

[59]A. F. Starace, Appl. Opt. **19**, 4051 (1980), and references therein.

[60]G. Wendin, and A. F. Starace, Phys. Rev. A **28**, 3143 (1983).

[61]G. Wendin, Phys. Scr. **16**, 296 (1977).

[62]Z. Crljen, and G. Wendin, Phys. Scr. **32**, 359 (1985), and references therein.

[63]F. A. Parpia, W. R. Johnson, and V. Radojević, Phys. Rev. A **29**, 3173 (1984).

[64]G. Wendin, *Extended Abstracts of the 6th International Conference on Vacuum Ultra-Violet Radiation Physics, Charlottesville, Virginia, 1980* (unpublished), Vol. II, p. II-87.

[65]V. Schmidt, S. Krummacher, F. Wuilleumier, and P. Dhez, Phys. Rev. A **24**, 1803 (1981).

[66]V. Schmidt, in *Proceedings of the Conference on X-ray and Atomic Inner-Shell Physics (University of Oregon, 1982),* AIP Conf. Proc. No. 94, edited by B. Crasemann (AIP, New York, 1982), p. 544.

[67]J. E. Hansen, and P. Scott, Phys. Rev. A **33**, 3133 (1986).

[68]G. Wendin, L. Jönsson, and A. L'Huillier, Phys. Rev. Lett. **56**, 1241 (1986); A. L'Huillier and G. Wendin, J. Phys. B **20**, L37 (1987).